Neuron

CellPress

Perspective

Ultra-slow Oscillations in fMRI and Resting-State Connectivity: Neuronal and Vascular Contributions and Technical Confounds

Patrick J. Drew,[1,2,3,8] Celine Mateo,[4,8] Kevin L. Turner,[2] Xin Yu,[5,6] and David Kleinfeld[4,7,*]
[1]Department of Engineering Science and Mechanics, Pennsylvania State University, University Park, PA 16802, USA
[2]Department of Biomedical Engineering, Pennsylvania State University, University Park, PA 16802, USA
[3]Department of Neurosurgery, Pennsylvania State University, University Park, PA 16802, USA
[4]Department of Physics, University of California, San Diego, La Jolla, CA 92093, USA
[5]High-Field Magnetic Resonance Department, Max Planck Institute for Biological Cybernetics, 72076 Tübingen, Germany
[6]MGH/MIT/HMS Athinoula A. Martinos Center for Biomedical Imaging, Department of Radiology, Harvard Medical School, Massachusetts General Hospital, Charlestown, MA 02114, USA
[7]Section of Neurobiology, University of California, San Diego, La Jolla, CA 92093, USA
[8]These authors contributed equally
*Correspondence: dk@physics.ucsd.edu
https://doi.org/10.1016/j.neuron.2020.07.020

SUMMARY

Ultra-slow, ~0.1-Hz variations in the oxygenation level of brain blood are widely used as an fMRI-based surrogate of "resting-state" neuronal activity. The temporal correlations among these fluctuations across the brain are interpreted as "functional connections" for maps and neurological diagnostics. Ultra-slow variations in oxygenation follow a cascade. First, they closely track changes in arteriole diameter. Second, interpretable functional connections arise when the ultra-slow changes in amplitude of γ-band neuronal oscillations, which are shared across even far-flung but synaptically connected brain regions, entrain the ~0.1-Hz vasomotor oscillation in diameter of local arterioles. Significant confounds to estimates of functional connectivity arise from residual vasomotor activity as well as arteriole dynamics driven by self-generated movements and subcortical common modulatory inputs. Last, methodological limitations of fMRI can lead to spurious functional connections. The neuronal generator of ultra-slow variations in γ-band amplitude, including that associated with self-generated movements, remains an open issue.

INTRODUCTION

How do brains compute? The answer to this question takes on many guises. It has proven useful to differentiate brain regions on the mesoscopic scale (i.e., as an average of a large number of individual neurons) and thus define connections and signaling on the same mesoscopic scale (Mitra, 2014; Zeng, 2018). As an example, the flow of sensory input in the transformation from perception to action can be described as a flow from primary sensory areas to motor areas (Ferezou et al., 2007; Li et al., 2016). Mesoscopic connectivity diagrams are readily determined based on the histological analysis of tissue subsequent to injection and transport of anterograde and/or retrograde markers (Bohland et al., 2009; Kim et al., 2017). However, determination of connectivity in a living animal and modulation of signaling along established axonal pathways as a function of brain state require a noninvasive procedure. A well-established but incompletely understood approach is based on functional magnetic resonance imaging (fMRI), an imaging modality that infers neuronal activity from changes in localized brain blood oxygenation (Logothetis and Wandell, 2004; Shulman et al., 2002).

Here we review the use of fMRI to infer neuronal connectivity between well-separated regions in the forebrain. These are correlation-based methods, and regions with strong correlations between their resting-state signals are said to be "functionally connected." Connected graphs that are comprised of regions as vertices and strong correlations as edges are said to form "default networks" of brain activity (Greicius et al., 2003; Raichle et al., 2001; Sporns et al., 2005). Such networks have been characterized in humans (De Luca et al., 2005, 2006; Majeed et al., 2011; Zhao et al., 2008), monkeys (Shmuel and Leopold, 2008; Vincent et al., 2007), and rats (Gozzi and Schwarz, 2016; Lu et al., 2012; Majeed et al., 2011; Stafford et al., 2014; Thompson et al., 2013), but not without controversy regarding reliability (Honey et al., 2009). Our review generally avoids the discussion of signals from anesthetized animals and humans in light of the strong disruption of the interaction between neurons and blood vessels by most anesthetic agents (Gao et al., 2017; Goense and Logothetis, 2008; Pisauro et al., 2013).

FUNDAMENTALS

The flow and oxygenation of blood in the brain are modulated by neuronal activity. This modulation forms the basis of fMRI and intrinsic optical signal (IOS) imaging. Two coupled effects are at work. First, an increase in neuronal activity will lead to an

Please cite this article in press as: Drew et al., Ultra-slow Oscillations in fMRI and Resting-State Connectivity: Neuronal and Vascular Contributions and Technical Confounds, Neuron (2020), https://doi.org/10.1016/j.neuron.2020.07.020

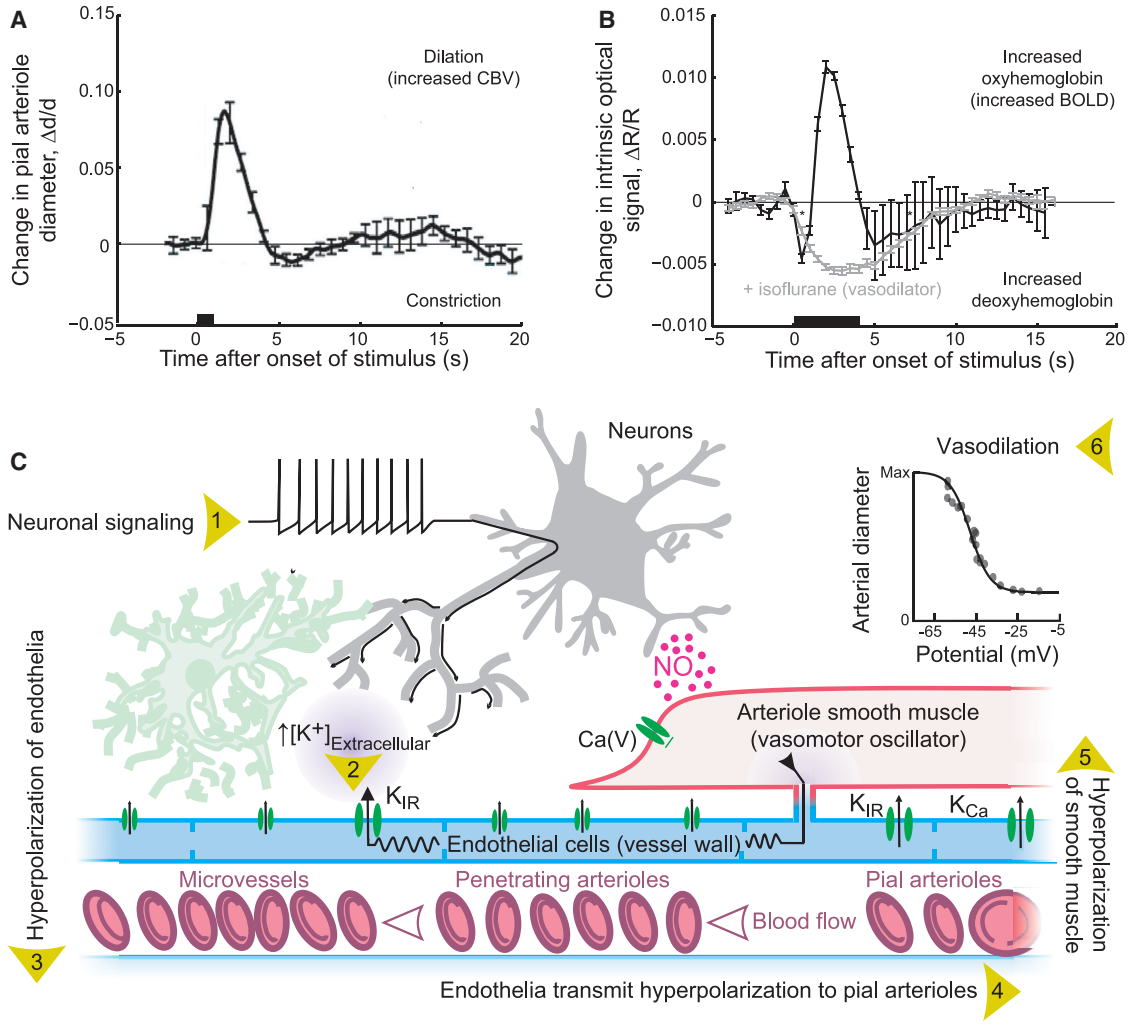

Figure 1. The Neocortical Vascular Response to Phasic Sensory Stimulation and the Mechanism for Fast Neurovascular Coupling

(A) The canonical effect of neuronal activity on the diameter of pial vessels as measured with two-photon laser-scanning microscopy (Kleinfeld et al., 1998) using a head-fixed mouse. The stimulus is a 500-ms puff to the vibrissae. The error bars are +/− one standard error of the mean (SEM). Adapted from Uhlirova et al. (2016).

(B) The canonical effect of neuronal activity on hemodynamics as measured with intrinsic optical imaging using 630-nm light (Grinvald et al., 1988) using a head-fixed mouse. The stimulus is a 4-s puff to the vibrissae. The isoflurane data refer to a breathing mixture of 1.8% (v/v) isoflurane in oxygen. The error bars are +/− SEM. Adapted from Knutsen et al. (2016).

(C) Rapid mechanisms for communication of neuronal activity to drive smooth muscle hyperpolarization and arteriole dilation. Neural activity (1) leads to an increase in K^+ in the perivascular space surrounding microvessels that activates the potassium inward rectifier (2), K_{IR}, to generate local hyperpolarization of the endothelial membrane (3). The hyperpolarization spreads to adjacent endothelial cells through gap junctions to activate K_{IR} currents in adjacent cells (4). This results in a propagating signal from microvessels to penetration arterioles and, finally, surface or pial vessels. The hyperpolarization spreads to adjacent smooth muscle cells (5) and deactivates voltage-dependent Ca^{2+} currents, Ca(V), to induce smooth muscle relaxation and arteriolar dilation (6). Rapid arteriole dilation is also induced by binding of nitric oxide (NO), which is released from some inhibitory neurons, as well as other brain cells (i.e., endothelial cells, astrocytes, and microglia). The increase in arteriole diameter (A) can lead to an increase in blood flow. Adapted from Longden et al. (2017) and Knot and Nelson (1998).

increase in the diameter of the pial arterioles that distribute blood to the brain. This change in diameter will long outlast the stimulus (Drew et al., 2011; Uhlirova et al., 2016; Figure 1A). Second, an increase in neuronal activity will initially lead to a decrease in blood oxygenation in the microvessels and veins, seen most prominently in the upper layers of the cortex (Buxton, 2001; Grinvald et al., 1991; Tian et al., 2010), but this interpretation is not universally accepted (Şencan et al., 2020; Sirotin et al., 2009; Uludağ et al., 2009). The increase in oxygen consumption is soon overcompensated by an increase in blood flow and a concomitant increase in blood oxygenation. The overcompensation reflects the active nature of neurovascular coupling (Attwell et al., 2010; Cauli and Hamel, 2010; Iadecola, 2004; Kleinfeld et al., 2011). The overcompensation can localize to one or a few cortical columns (Grinvald et al., 1991), but it may have a global component from dilation of arterioles caused by change in the activity of sympathetic input (Dacey and Duling, 1984).

The oxygenation state of blood can be detected via differences in the electronic properties of oxy- versus deoxyhemoglobin. This is reported by a greater reflection of red light by

Please cite this article in press as: Drew et al., Ultra-slow Oscillations in fMRI and Resting-State Connectivity: Neuronal and Vascular Contributions and Technical Confounds, Neuron (2020), https://doi.org/10.1016/j.neuron.2020.07.020

CellPress

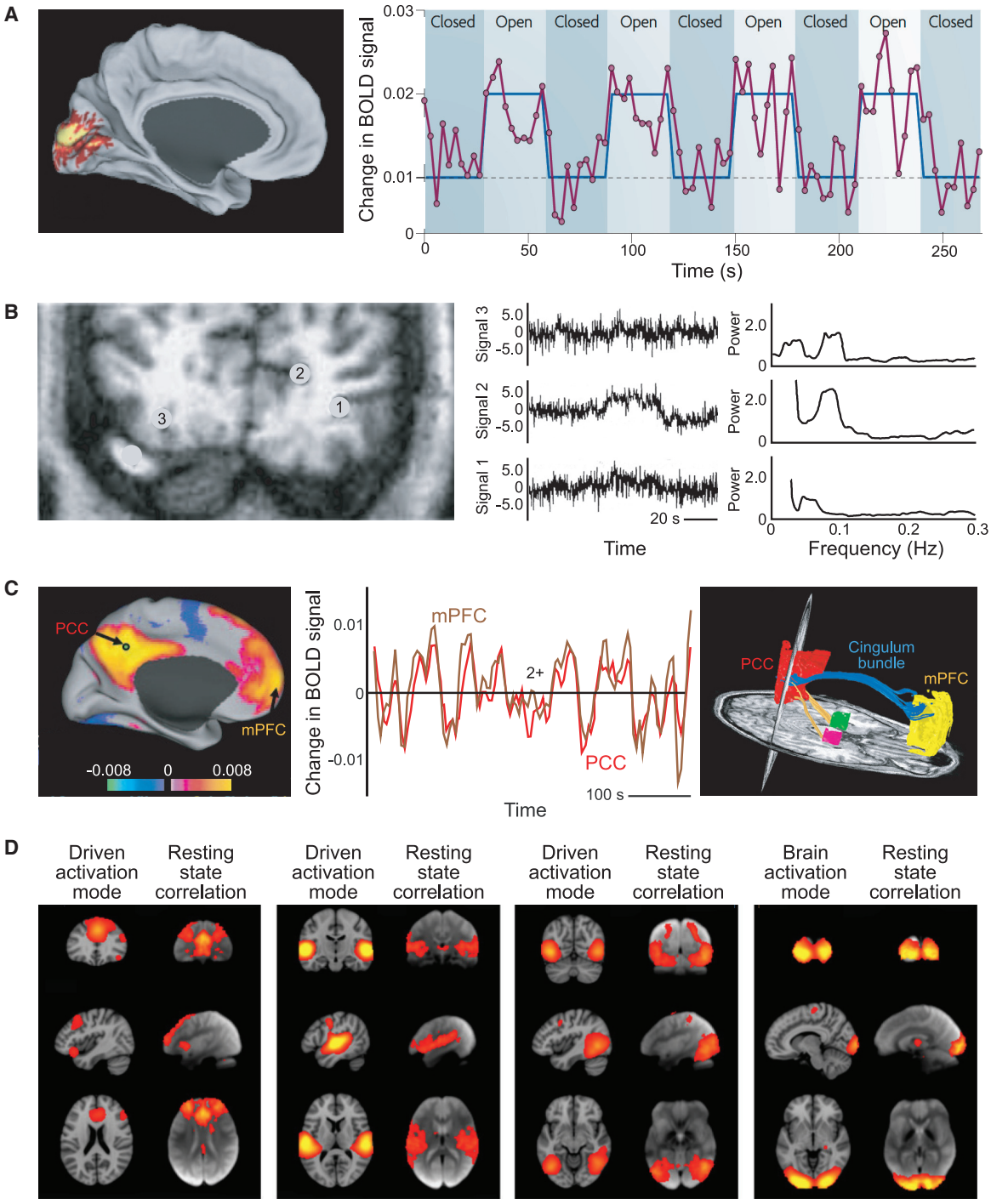

Figure 2. Functional MRI (fMRI) Uses Correlations in the Fluctuations of Signal Strength to Infer Brain Regions that Are Directly Connected

(A) Changes in the basic blood-oxygen-level-dependent (BOLD) fMRI signals generated in the human visual cortex in response to changes in luminance in a full-field visual input. The unaveraged BOLD signal (magenta) was obtained from a region in the primary visual cortex during a task that required subjects to open and close their eyes. The task is shown in blue, and the times are delayed to account for the hemodynamic response. The subtraction of the eyes-closed condition from the eyes-open condition identifies a BOLD signal intensity difference in the primary visual cortex (shown on the right). Note the variability as well as the average increase in signal amplitude upon stimulation. From Fox and Raichle (2007).

(B) BOLD fMRI signals were obtained from a coronal slice, 2.8 cm from the occipital pole (left). Shown are three unprocessed time courses of the BOLD fMRI signal of representative voxels, numbered 1–3 and located outside of the visual cortex, and their corresponding frequency spectra (right). A binocular visual stimulus, provided by a pair of flickering red LED patterns, was on during the 40- to 70-s time interval of the 110-s period and drives voxel 4 (data not reproduced here). From Mitra et al. (1997).

(legend continued on next page)

Please cite this article in press as: Drew et al., Ultra-slow Oscillations in fMRI and Resting-State Connectivity: Neuronal and Vascular Contributions and Technical Confounds, Neuron (2020), https://doi.org/10.1016/j.neuron.2020.07.020

oxy- versus deoxyhemoglobin, which is routinely detected by IOS imaging (Lieke et al., 1989; Figure 1B). It is also reported by a change from a diamagnetic to a paramagnetic state by oxy- versus deoxyhemoglobin, respectively (Pauling and Coryell, 1936). Thus, the magnetic susceptibility of capillary and venous blood is correlated with neuronal activity. The changes in arteriole diameter and blood oxygenation are coupled; the overcompensation of blood oxygenation is quenched when the pial arterioles are fully dilated using isoflurane prior to onset of neuronal activity (Figure 1B; Knutsen et al., 2016; Vazquez et al., 2012).

Communication from Neurons to Arteriole Smooth Muscle

How do neurons communicate with arterioles? There are multiple mechanisms neurons in the brain use to control their own supply of blood (Attwell et al., 2010; Cauli and Hamel, 2010; Iadecola, 2004; Kleinfeld et al., 2011). We review two mechanisms that act on a less than 1 s timescale. The lumen of the blood vessels is formed by endothelial cells that are connected by relatively low-resistance gap junctions so that passive signaling occurs with an ~2-mm electrotonic length (Segal and Duling, 1989; Welsh et al., 2018). Further, the smooth muscle cells that drive vascular tone are in strong electrical contact with the endothelial cells. In the presence of bursts of neuronal spikes, there is an outflow of K^+ ions in the perivascular space (Caesar et al., 1999; Rasmussen et al., 2019). This can lead to regenerative, hyperpolarizing pulses that propagate along the endothelial cells from subsurface microvessels to penetrating arterioles (Longden et al., 2017; Moshkforoush et al., 2020) and then to pial arterioles (Figure 1C). The hyperpolarization spreads to smooth muscle and dilates the pial arterioles (Filosa et al., 2006; Knot and Nelson, 1998; Figure 1C, inset). This sequence of activation is supported by the stimulus-driven progression in arteriole dilation from middle layers to the pia in the cortex (Tian et al., 2010). Although details of the conditions for passive versus active spread of signals in the pial network remain to be addressed (Harraz et al., 2018), electrical coupling through the endothelium provides a means for neurons to directly influence the diameter of neighboring arterioles (Figure 1A).

Nitric oxide (NO) is a well-known vasodilator produced by NO synthase (NOS) in neurons and can act quickly to relax smooth muscle (Figure 6). As a caveat, the role of NO as a transient actuator of change in arteriole dilation (Ma et al., 1996), as opposed to a co-factor in effecting change (Lindauer et al., 1999), remains unsettled (Attwell et al., 2010), although optogenetic stimulation of neurons that express NOS drives an increase in blood flow (Krawchuk et al., 2019). The role of astrocytes in the control of flow is also controversial (Kleinfeld et al., 2011; Mishra et al., 2016; Nizar et al., 2013; Rosenegger et al., 2015), with arteriole dilation occurring only in the presence of relatively large signaling events by astrocytes (Schulz et al., 2012).

Background on fMRI

The blood-oxygen-level-dependent (BOLD) fMRI signal exploits the shift in the magnetic properties of deoxyhemoglobin versus oxyhemoglobin (Villringer and Dirnagl, 1995). In practice, these are detected by changes in the relaxation time of water protons in the brain (Ogawa et al., 1993; Stephan et al., 2004). Longer relaxation times imply greater oxygenation and a larger BOLD fMRI signal. The BOLD effect was discovered in 1990 by Ogawa et al. (1990) using anesthetized rats. Two years later, BOLD was demonstrated independently in the awake human brain by Bandettini et al. (1992), Kwong et al. (1992), and Ogawa et al. (1992). As an example, successive eye opening and closing in humans leads to a change in the BOLD fMRI signal in the brain region that corresponds to the primary visual cortex (Fox and Raichle, 2007; Figure 2A). In terms of impact, use of BOLD fMRI has stormed across the disciplines of psychology and cognitive neuroscience as a means to infer changes in neuronal activity during all aspects of cognitive tasks performed by humans.

A complementary technique, cerebral blood volume (CBV) fMRI, infers neuronal activity from an increase in total hemoglobin in response to neuronal activity. It was first demonstrated in the human brain using subjects whose blood was doped with gadolinium, a paramagnetic ion that vastly increases the magnetic susceptibility of blood (Belliveau et al., 1991; Kwong et al., 1992). The increase in blood volume is secondary to an increase in arteriole diameter (Figure 1B). Subsequent work has demonstrated CBV fMRI using label-free procedures (Huber et al., 2017; Lu et al., 2003).

Noise and Determination of Correlated Brain Activity

The physicist Lewis Branscomb famously wrote "God loves the noise as much as the signal" (Branscomb, 1995). The noise in the fMRI signal, a part of physiological contributions such as breathing and technical noise, has dominant but broad spectral bands (Mitra and Bokil, 2008; Papoulis, 1962) near 0.1 Hz (Figure 2B). The exact frequency can vary on the scale of centimeters across the human brain. Mindful of Branscomb's prescient comment, only a few years after the advent of BOLD fMRI, experiments in the laboratory of James Hyde showed that the variability observed in the BOLD fMRI signal is correlated across well-separated regions in the brain. The initial observations involved subregions in the motor cortex of the two hemispheres whose BOLD fMRI signals co-fluctuate in the vicinity of 0.1 Hz in the absence of a task (Biswal et al., 1995). These signals, in contrast to stimulus- and task-based fMRI, are measured in the absence

(C) The BOLD fMRI signals recorded from two distant regions in the human cortex, the posterior cingulate/precuneus cortex (PCC) and the medial prefrontal cortex (mPFC), are highly correlated on a timescale of tens to hundreds of seconds. Correlations are calculated between a seed voxel in the PCC and all other voxels in the brain for a single subject during rest. The spatial distribution of correlation coefficients shows positive and negative values and was thresholded at $R^2 = 0.1$ (left image). The time course for a single run is shown for the seed region (PCC) and a region (mPFC) positively correlated with this seed region. The functional connection between the PCC and the mPFC is consistent with a fiber track revealed by diffusion tensor imaging (blue trace in the right image). Left and center panels from Fox et al. (2005); right panel from Greicius et al. (2009).

(D) Four well-matched pairs of resting-state subnetworks that show a close correspondence between the independent analyses of activated (left column) and resting-state (right columns) brain dynamics. Activation data are from the 20-component analysis of the 29,671-subject BrainMap activation database (Fox and Lancaster, 2002; Laird et al., 2005), and resting-state data are from a separate analysis of a 36-subject resting-state fMRI dataset (Smith et al., 2009). Shown are the three most informative orthogonal slices for each pair. Left columns: network from BrainMap, shown superimposed on the MNI152 standard space template image. Right columns: resting-state fMRI data, shown superimposed on the mean fMRI image from all subjects. From Smith et al. (2009).

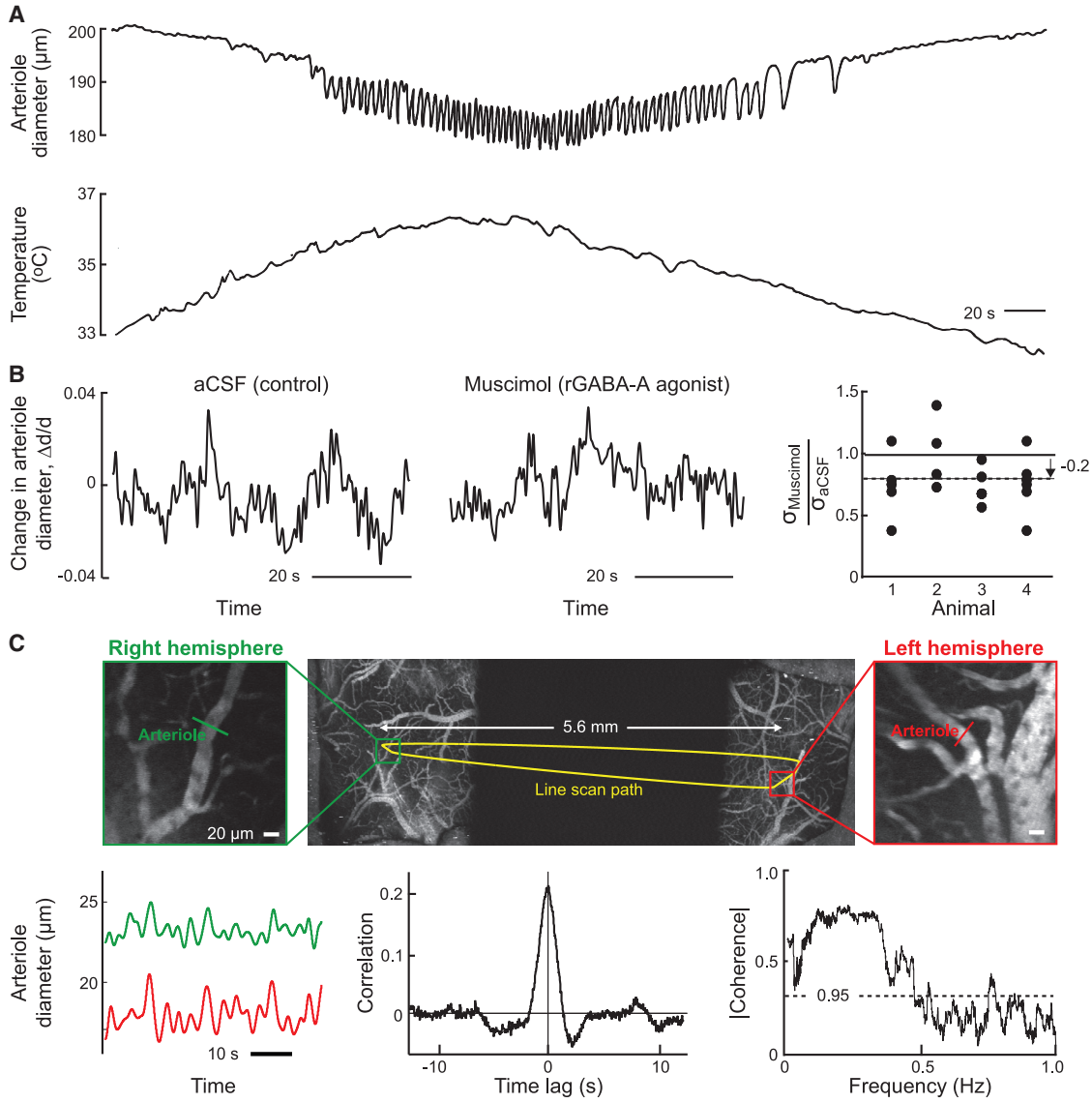

Figure 3. *In Vitro* and *In Vivo* Measurements of Vasomotion, a Rhythmic Change in Arteriole Diameter with a Broad-Band Intrinsic Frequency Centered Near 0.1 Hz

(A) Simultaneous recording of lumen diameter (top) and temperature (bottom) in a cerebral artery that was isolated from a spontaneously hypertensive, stroke-prone rat and pressurized to 80 mmHg. Diameter oscillations appear when the artery is warmed above 35°C. From Osol and Halpern (1988).

(B) Example of normalized diameter measurements from a single pial arteriole with two-photon laser-scanning microscopy following local artificial cerebrospinal fluid (aCSF) infusion (left) and muscimol infusion (center) in a single animal. Shown is a population summary of the root-mean-square deviation in pial arteriole diameter after muscimol infusion (19 vessels from 4 animals); oscillation amplitudes were reduced following infusion of muscimol compared with aCSF. From Winder et al. (2017).

(C) Two-photon imaging of vasomotion in cortical arterioles across both hemispheres of an awake, head-fixed mouse. A maximally projected image stack across 500 μm of the preparation was obtained with ultra-large field-of-view two-photon microscopy (Tsai et al., 2015) (top row); the dark region in the middle corresponds to a physical mask. The arbitrary line scan path of the beam (yellow) spans both hemispheres. The expanded images (center row) are single planes in each hemisphere and serve to highlight the path of the line scan through individual vessels whose diameters were concurrently monitored. Vasomotor oscillations measured simultaneously from pial arteries in the right (green) and left (red) hemispheres appear synchronous (center panel in center layer). The full dataset of 600 s is seen to be correlated with a lag time at the peak of 0.0 ± 0.1 s (lower row, left panel). The spectral coherence in the diameter from the same pair of arterioles was calculated with a bandwidth of 0.04 Hz. From Tsai et al. (2015).

of a cognitive task or any overt stimulus and are referred to as resting-state fMRI signals (Biswal et al., 2010). In fact, the signal between any pair of well-separated regions in the brain will co-fluctuate so long as they maintain long-range (i.e., white matter) connections (Fox et al., 2005). This is illustrated for resting-state BOLD fMRI signals from the posterior cingulate/precuneus cortex (PCC) and medial prefrontal cortex (mPFC) (Figure 2C, left and center), which are connected by a white matter tract along

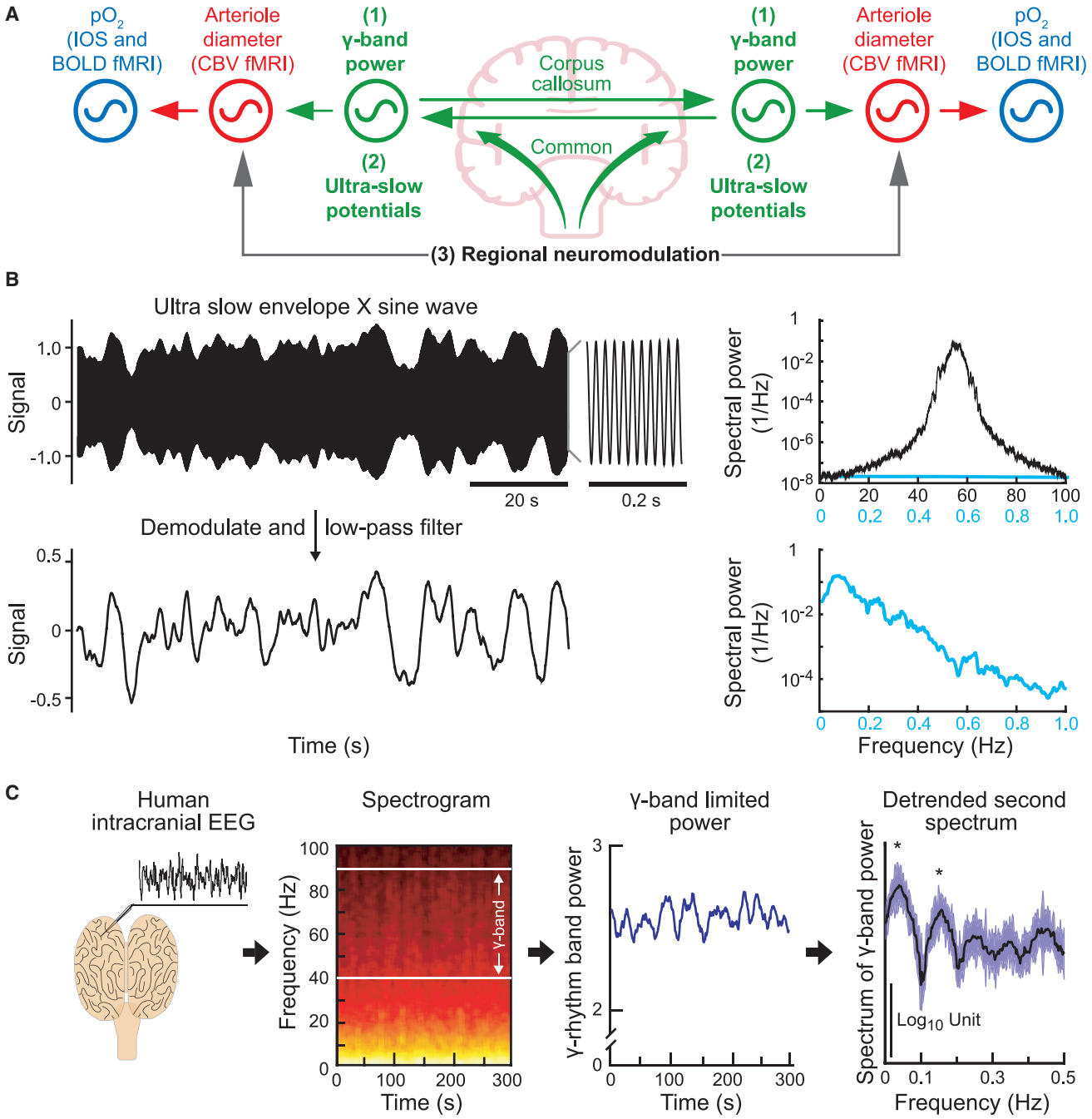

Figure 4. Ultra-slowly Varying Neuronal Signals Have Multiple Potential Origins but Are Predominantly Encoded by the Ultra-slow Modulation of the Fast γ-Band Oscillations

(A) Coupled oscillator model for resting-state neurovascular coupling. Shown are the three potential coupling mechanisms for entrainment of vasomotor oscillations across separate regions of the brain: (1) the ultra-slow envelope of the γ-band oscillations shared across separate regions, as illustrated in (B); (2) ultra-slow electrical potentials per se that are shared across separate regions; and (3) region-specific neuromodulation of brain activity. Adapted from Mateo et al. (2017).

(B) A model to illustrate amplitude modulation using an ultra-slow signal to modulate a fast underlying oscillatory signal. The top trace is the product of a carrier centered at $f\gamma$ = 55 Hz and a 0.1- to 0.2-Hz band-limited noise source for the ultra-slow modulate. The associated spectrum was computed with a bandwidth of 0.5 Hz (black trace) or 0.05 Hz (blue trace). The bottom trace shows the frequency components of the ultra-slow envelope after demodulation and low-pass filtering to remove signals near $2f_{\gamma}$. The associated spectrum was computed with a bandwidth of 0.05 Hz. From Mateo et al. (2017).

(legend continued on next page)

Please cite this article in press as: Drew et al., Ultra-slow Oscillations in fMRI and Resting-State Connectivity: Neuronal and Vascular Contributions and Technical Confounds, Neuron (2020), https://doi.org/10.1016/j.neuron.2020.07.020

the cingulum bundle (Greicius et al., 2009) (Figure 2C, right). In general, resting-state fMRI signals are particularly strong between regions in opposing hemispheres with mirrored neuronal activation (Smith et al., 2009; Figure 2D), but these signals are accompanied by brain-wide activation (Schölvinck et al., 2015).

The Arteriole Diameter Naturally Oscillates Near 0.1 Hz

What are the physiological attributes of blood vessels that allow them to be coupled to ongoing neuronal activity in the absence of a task (Figures 2C and 2D) as opposed to be driven by strong sensory stimuli (Figure 1)? Further, what is the origin of the ~0.1-Hz frequency scale for the ultra-slow dynamics that dominate the resting-state BOLD fMRI signal (Figure 2B)? Both of these questions are answered by recalling that arteries undergo vasomotor oscillations as part of their normal physiology (Intaglietta, 1990). These are collective oscillations of contractile tone in the smooth muscle cells that surround arterioles and lead to rhythmic changes in arteriole diameter (Aalkjær et al., 2011; Intaglietta, 1990), referred to as vasomotion. The rhythm is thought to be generated by the interactions of active conductances in the membranes of smooth muscle and endothelial cells (Aalkjaer and Nilsson, 2005; Haddock and Hill, 2005) with the mechanical forces generated by flow (Koenigsberger et al., 2006; Stergiopulos et al., 1998). Vasomotion occurs within a broad frequency band that is centered near 0.1 Hz in humans (Noordmans et al., 2018; Obrig et al., 2000; Rayshubskiy et al., 2014), mice (Drew et al., 2011), and rats (Kleinfeld et al., 1998; Mayhew et al., 1996). Vasomotor oscillations in arteriole diameter drive oscillations in the velocity of red blood cells in microvessels (Drew et al., 2010; Kleinfeld et al., 1998) and changes in oxygenation of brain tissue (Mateo et al., 2017; Mayhew et al., 1996),

As an intrinsic property, vasomotor oscillations are observed in isolated brain arterioles that are cannulated, pressurized, and maintained at physiological temperature (Osol and Halpern, 1988; Figure 3A). Critically, vasomotion is observed in pial arterioles *in vivo* (Figure 3B, left) and is only slightly reduced in amplitude, by a factor of 0.2, when cortical activity is silenced to isolate the vessels from ongoing cortical, but not sympathetic, neuronal activity (Winder et al., 2017; Figure 3B, center and right).

The presence of ultra-slow natural oscillations in the diameter of brain arterioles raises three questions. First, what is the relation of the oscillation to the change in oxygenation of the neighboring tissue; i.e., the parenchymal contribution to the BOLD signal? Simultaneous measurements of arteriole diameter and the IOS in awake mice show that the two are strongly coherent (Mateo et al., 2017). The peak value of oxygenation lags the peak of vasodilation by ~1 s. The positive coupling of blood oxygenation with a change in arteriole diameter is consistent with the changes that occur upon sensory stimulation (Figure 1).

The second question, given the coupling of blood oxygenation to vasomotion, concerns the spatial scale of synchronous vasomotor oscillations. The results from direct measurements of vessel diameter in awake rodents indicate that vessels within a radius of ~2 mm tend, on average, to dilate synchronously (Mateo et al., 2017). Further, because the radius is the only dimension of blood vessels that can change, CBV fMRI provides a measure of arteriole diameter. Using this technique with anesthetized rodents, a correlation length of ~2 mm has also been reported (He et al., 2018). Thus, despite the short-range falloff, are changes in diameter strongly coordinated across distant but mirrored regions in the two hemispheres? Optical imaging data from rodents show that such transhemispheric changes are strongly correlated (Figure 3C; Mateo et al., 2017; Tsai et al., 2015). Similar results are inferred with CBV fMRI of the primate brain (Schölvinck et al., 2010). All told, mirrored regions in the two hemispheres show synchronous oscillations in arteriole diameter (Figure 3C) in addition to blood oxygenation (Figure 2D).

The third question is how fast the callosal coupling between neurons in opposite hemispheres must be to support synchronous ultra-slow activity. For the simplest models of weakly coupled oscillators, this means a delay of less than a quarter of a period (Sompolinsky et al., 1991; Yeung and Strogatz, 1999). This corresponds to ~2 s, which is two orders of magnitude longer than transhemispheric propagation delays. The arteriole vasomotion in each hemisphere is synchronous through the similarly delayed neuronal-to-vascular coupling (Figure 1).

SOURCES OF ULTRA-SLOW ELECTRICAL SIGNALING TO COUPLE TO VASOMOTION

The theory of weakly coupled oscillators (Kuramoto, 1984) implies that vasomotor oscillations can phase-lock to rhythmic neuronal activity within the same ~0.1-Hz frequency band. We consider three such sources of activity (Figure 4A). The first two involve ultra-slow variations in neuronal electrical potential. One realization is in terms of an ultra-slowly varying envelope of high-frequency electrical oscillations in the brain (Leopold et al., 2003; Nir et al., 2008; Thompson et al., 2013). A second is in terms of potential ultra-slow variations in the electrocorticogram (ECoG) or electroencephalogram (EEG) (He and Raichle, 2009). The ECoG and EEG measure spatially extended and temporally coherent extracellular current flow in the brain (Lemon, 1984). The third potential source of ultra-slow rhythmic activity is neuromodulator nuclei. We consider the viability of each of these signaling mechanisms as a prelude to describing the locking of vasomotor activity to ultra-slow electrical signal in the brain.

Ultra-slow Electrical Signaling by Modulation of γ-Band Oscillations

Gamma-band oscillations refer to rhythmic brain activity in a broad range of frequencies, typically 30–80 Hz. It can be

(C) Measurements and analysis of ultra-slow variations in the power of the surface ECoG during stage 2 sleep in a human subject (left panel); from Nir et al. (2008). The spectrogram of the ECoG shows the slow variation in power in the 40- to 90-Hz γ-band (left-of-center panel); window of 10 s, bandwidth of 1.5 Hz, and color scales of the logarithm of power from black (low) to yellow (high). The time series of the variation of integrated power in the γ-band of the ECoG shows oscillations on the 10-s timescale. The spectrum of the derivative of this time series, a procedure that removes a power $\propto 1/f^2$ trend from the spectrum, has statistically significant peaks at frequencies near ~0.1 Hz. The error bars are +/− SEM and the stars indicate significance at p=0.01. Reanalysis from Drew et al. (2008).

Please cite this article in press as: Drew et al., Ultra-slow Oscillations in fMRI and Resting-State Connectivity: Neuronal and Vascular Contributions and Technical Confounds, Neuron (2020), https://doi.org/10.1016/j.neuron.2020.07.020

generated *in vitro* by networks of solely fast-spiking inhibitory neurons (Whittington et al., 1995), consistent with theoretical predictions (Hansel et al., 1993; Van Vreeswijk et al., 1994). *In vivo*, the details of the oscillatory waveform are shaped by the interactions between parvalbumin and pyramidal neurons (Cardin et al., 2009; Sohal et al., 2009) as well as by interactions with different classes of inhibitory neurons (White et al., 2000) and cholinergic modulation (Pinto et al., 2013).

A key feature of γ-band oscillations is that the amplitude or, equivalently, the spectral power can vary over time (Leopold et al., 2003; Liu and Duyn, 2013; Mateo et al., 2017; Nir et al., 2008; Thompson et al., 2013). In fact, an increase in power in the γ-band is a predictor of a subsequent increase in arteriole diameter and blood oxygenation (Mateo et al., 2017; Winder et al., 2017). Consistent with these physiological changes, there is a corpus of evidence that increased power in the γ-band correlates with an increase in the BOLD fMRI signal (Goense and Logothetis, 2008; Keller et al., 2013; Lachaux et al., 2007; Lima et al., 2014; Niessing et al., 2005; Nir et al., 2007; Schölvinck et al., 2010). Although the power in the γ-band is the best predictor of an increase in arteriole diameter, the correlation with spectral power extends down to lower frequencies (Goense and Logothetis, 2008; Mateo et al., 2017; Winder et al., 2017).

As a matter of principle, amplitude modulation (Black, 1953) provides a means for ultra-slow signals to be transmitted in the brain, as can occur by modulating the interspike interval in a spike train by an inhomogeneous spike rate (Okun et al., 2019). Here the γ-rhythm oscillations serve as the underlying carrier frequency, and the broad-band, ~0.1-Hz rhythm modulates the amplitude of the γ-rhythm oscillations (Figure 4B). The power spectrum of the γ-rhythm oscillations is broadened by the modulation but still centered at a high frequency; there is no spectral power at the broad-band, ~0.1-Hz modulation (Figure 4B). Demodulation of the signal, which involves spectral mixing and can be accomplished by the threshold properties of neurons (Ahrens et al., 2002), retrieves the ultra-slow signal (Figure 4B). Recent data from the mouse accessory olfactory bulb imply that ultra-slow modulation can be quite strong in practice (Tsitoura et al., 2020).

Evidence of encoding of ultra-slow oscillations by modulation of γ-rhythm oscillations comes from studies on monkeys (Leopold et al., 2003) and human subjects (Nir et al., 2008). The human study involved bilateral recordings of multi-unit spike waveforms and the ECoG from the parietal and temporal lobes of both cortices in pre-operative patients. A spectrogram of the ECoG acquired while a subject was in non-rapid eye movement sleep shows that the power in the γ-band is modulated slowly (Figure 4C). The spectral power of the modulation in γ-band power, the so-called second spectrum, shows peaks at frequencies near 0.1 Hz (Drew et al., 2008; Figure 4C). These modulations are present during states of sleep and states of wakefulness.

Is the modulation in γ-band power correlated across hemispheres, as would be expected if these signals relate to transhemispheric correlation in the BOLD fMRI signal (Figure 2D) and arteriole diameter (Figure 3C)? The spike times at spatially adjacent regions as well as at functionally linked areas of opposing hemispheres are not coincident. In contrast, there is significant coherence in modulation of the spike rate and in the power of γ-band oscillations in the ECoG across sites in opposing hemispheres (Nir et al., 2008). During rest, there is a relatively large and positive correlation coefficient of 0.6 between ultra-slow ECoG signals from contralateral auditory areas compared with smaller correlation coefficients between signals from auditory and nonauditory areas. The stimulus-linked synchrony between the auditory areas in opposite hemispheres is likely mediated through callosal connections (Engel et al., 1991). The literature therefore suggests that ~0.1-Hz signals are transmitted as a modulation of the high-frequency γ-band rhythm, which is coherent across mirrored regions in the two hemispheres.

A final concern is the spatial specificity of the ultra-slow modulation that forms correlated signals across hemispheres. This was addressed using wide-field optical imaging of the dorsal surface of the cortex in transgenic mice that express functional indicators of intracellular calcium (Barson et al., 2020; Ma et al., 2016; Vanni et al., 2017) or transmembrane voltage (Chan et al., 2015; Mohajerani et al., 2013). These indicators report the accumulation of spiking activity, which approximates rectification of neuronal activity above a threshold level (Figure 4B) and thus reports the ultra-slow envelope of neuronal activity. Although strong correlations occur for frequencies over a range from 0.1–10 Hz, the amplitude of the oscillations across the dorsal surface is greatest in the 0.08- to 0.16-Hz frequency band (i.e., centered near 0.1 Hz) as opposed to bands below this frequency and up to 10 Hz (Vanni et al., 2017). Further, bilateral symmetry of the neuronal response is largely reduced in acallosal mice (Mohajerani et al., 2010), but this issue is not without controversy (Quigley et al., 2003; Tyszka et al., 2011).

Ultra-slow Changes in the ECoG Report Non-neuronal Dynamics

The EEG is traditionally recorded as surface potentials across the brain (Lemon, 1984). Ultra-slow variations in the ECoG or EEG, also referred to as "DC potentials," are presumed to result from ultra-slow changes in active membrane currents (Besson et al., 1970) and are a complementary means to support ultra-slow neuronal activity to that of modulation of the high-frequency γ-rhythm (Figures 4B and 4C). However, extensive experimental evidence has shown that EEG signals with spectral components below ~1 Hz have a non-neuronal origin. One mechanism to generate ultra-slow surface potentials is through changes in the volume of blood in the brain. The electrical potential of the blood is negative relative to that of cerebrospinal fluid (Held et al., 1964; Sorensen and Severinghaus, 1970). Thus, dilation of arterioles, which, in the awake animal can take place over seconds, and dilation of veins, which can occur over tens of seconds (Drew et al., 2011; Huo et al., 2015; Pisauro et al., 2013), generates ultra-slow changes in the EEG (Besson et al., 1970; Nita et al., 2004; Vanhatalo et al., 2003; Voipio et al., 2003) that are unrelated to neuronal activity per se.

Experiments on human subjects have shown that a shift in blood volume, driven by changes in posture or breathing that are unlikely to induce significant neuronal effects, drive ultra-slow changes in the EEG. In the Mueller maneuver, the subject attempts to inhale with their mouth closed and nostrils plugged. In the Valsalva maneuver, the subject attempts to exhale against

Please cite this article in press as: Drew et al., Ultra-slow Oscillations in fMRI and Resting-State Connectivity: Neuronal and Vascular Contributions and Technical Confounds, Neuron (2020), https://doi.org/10.1016/j.neuron.2020.07.020

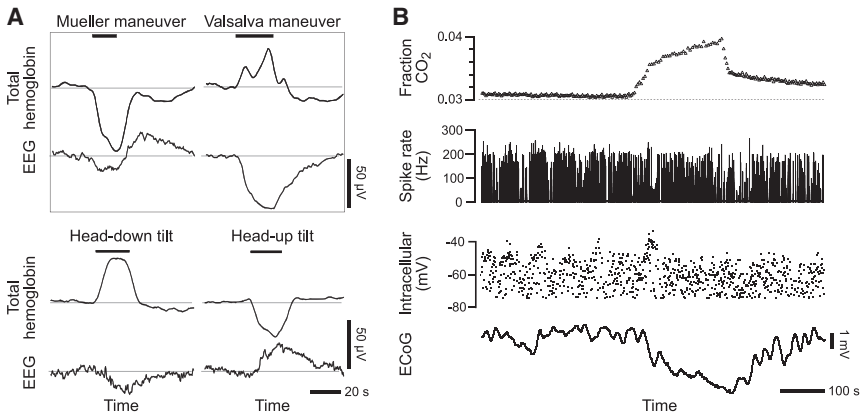

Figure 5. Ultra-slowly Varying Extracellular Potentials (DC Potentials) Can Have a Non-neuronal Origin

(A) Four changes in human body position that alter CBV, Mueller and Valsalva maneuvers and head tilt maneuvers, drive changes in EEG potential, as measured with scalp electrodes. The change in total blood volume was found from near-infrared absorption of brain blood perfusion using scalp emitters and detectors (Ichikawa et al., 1999). The EEG scalp-electrodes were at the 10–20 international coordinates Cz - (T3 + T4) for Mueller and Valsalva, Fz - (right mastoid) for head up, and Cz - (right mastoid) for head down. From Vanhatalo et al. (2003).

(B) Inhalation of CO_2, a vasodilator, drives a large shift in ECoG potentials with no effect on the transmembrane potential or spike rate of a simultaneously recorded neuron. Shown are intracellular and DC ECoG recordings during recurrent spike-wave seizures and hypoventilation in a cat under ketamine-xylazine anesthesia. From Nita et al. (2004).

a closed airway; this is a common means to equalize pressure to the sinuses. These procedures drive a change in blood volume, measured with near-infrared spectroscopy (NIRS), along with relatively large-amplitude EEG signals that follow the change in blood volume (Vanhatalo et al., 2003; Figure 5A). Tilting the head up or down (Figure 5A) as well as compression of the jugular vein give similar results (Vanhatalo et al., 2003). Complementary experiments that involve vasodilation support the hypothesis that slow potentials are generated by a change in blood volume. In particular, inhalation of carbon dioxide causes vasodilation on a timescale of minutes (Besson et al., 1970; Ngai and Winn, 1996) and leads to concurrent changes in the EEG signal in the less than 1 Hz frequency range (Voipio et al., 2003).

The gold standard in these neurovascular studies is to record slow changes in the ECoG that are induced by vasodynamics concurrent with the electrical activity of nearby neurons. Such studies were performed with cats, in which the CO_2 content of the inhalation gas could be altered to induce vasodilation (Nita et al., 2004). Consistent with a vascular but not a neuronal origin of ultra-slow electrical signals, simultaneous intracellular recordings from neurons (Figure 5B) and astrocytes show that the ultra-slow ECoG signals are not reflected in the neuronal or astrocyte membrane potential (Nita et al., 2004). Further, extracellular measurements as a function of depth in the cortex failed to find a reversal of the polarity of the ultra-slow signals with cortical depth, inconsistent with a synaptic origin of these potentials (Nita et al., 2004). *In toto*, the data refute the notion that ultra-slow neuronal signals are present in ultra-slow, brain-wide ECoG signals as opposed to the modulatory signal of the high-frequency γ-band carrier seen in the ECoG.

Are there other neuronal origins of ultra-slow electrical activity? Intracellular neuronal currents with variation in the ~1-Hz range have been described (Steriade et al., 1993), but there are no reports of slower ionotropic currents, with the exception of nicotinic acetylcholine receptors, which contain the α7 and β2 receptor subunits. These subunits may play an important role in generation of ultra-slow fluctuations in the spike rates of neurons in the frontal cortex (Koukouli et al., 2016). Other ion channels show depolarization-induced changes in recovery times that last up to hundreds of seconds (Toib et al., 1998), and spontaneous synaptic release shows correlations over a multiplicity of long timescales (Lowen et al., 1997). Although currents that rely on reaction-diffusion kinetics and concentration-dependent rates can be quite slow, they are not *a priori* oscillatory in nature.

Targeted Neuromodulatory Input to the Cortex

There is evidence that slow signals from cholinergic modulatory centers provide brain-wide modulation of the γ-rhythm (Turchi et al., 2018). The composite evidence also suggests that cholinergic signaling activates the M5 metabotropic pathway (Yamada et al., 2001) in penetrating arterioles (Adachi et al., 1992; Hotta et al., 2013; Sato et al., 2001; Vaucher and Hamel, 1995). Several studies have shown that projections from the basal forebrain, which contains a prominent cholinergic center, are targeted to specific brain regions (Kim et al., 2016a; Saper, 1984; Wu et al., 2014; Zaborszky et al., 2015). In particular, cholinergic targeting is specific at least down to the level of primary sensory areas (Kim et al., 2016a), consistent with the murine projectome of the basal forebrain (Li et al., 2018). Some cholinergic neurons could co-target functionally related areas (Li et al., 2018), but finer-scale organization, like retinotopy, may not be present (Huppé-Gourgues et al., 2018). The inputs to basal forebrain neurons also show targeted input from different brain regions (Gielow and Zaborszky, 2017).

The neuromodulator noradrenaline, released by projections from the *locus coeruleus*, also functions to change brain-wide behavior. Chemogenetic activation of the *locus coeruleus* leads to an increase in functional connectivity, as determined from the pairwise cross-correlations among signals from different brain regions (Zerbi et al., 2019). However, unlike for basal forebrain input, the projections from the *locus coeruleus* appear to be cortex wide and diffuse, with no evidence of regional projections (Kim et al., 2016a). Of interest, noradrenaline release leads to global activation as a function of the cognitive task (Cardoso et al., 2019).

We conclude that vasomotion could, in principle, phase lock to slow variations in neuromodulation. Only cholinergic modulatory input has the regional specificity that suggests feasibility, but even for this case there is no evidence of changes in modulation

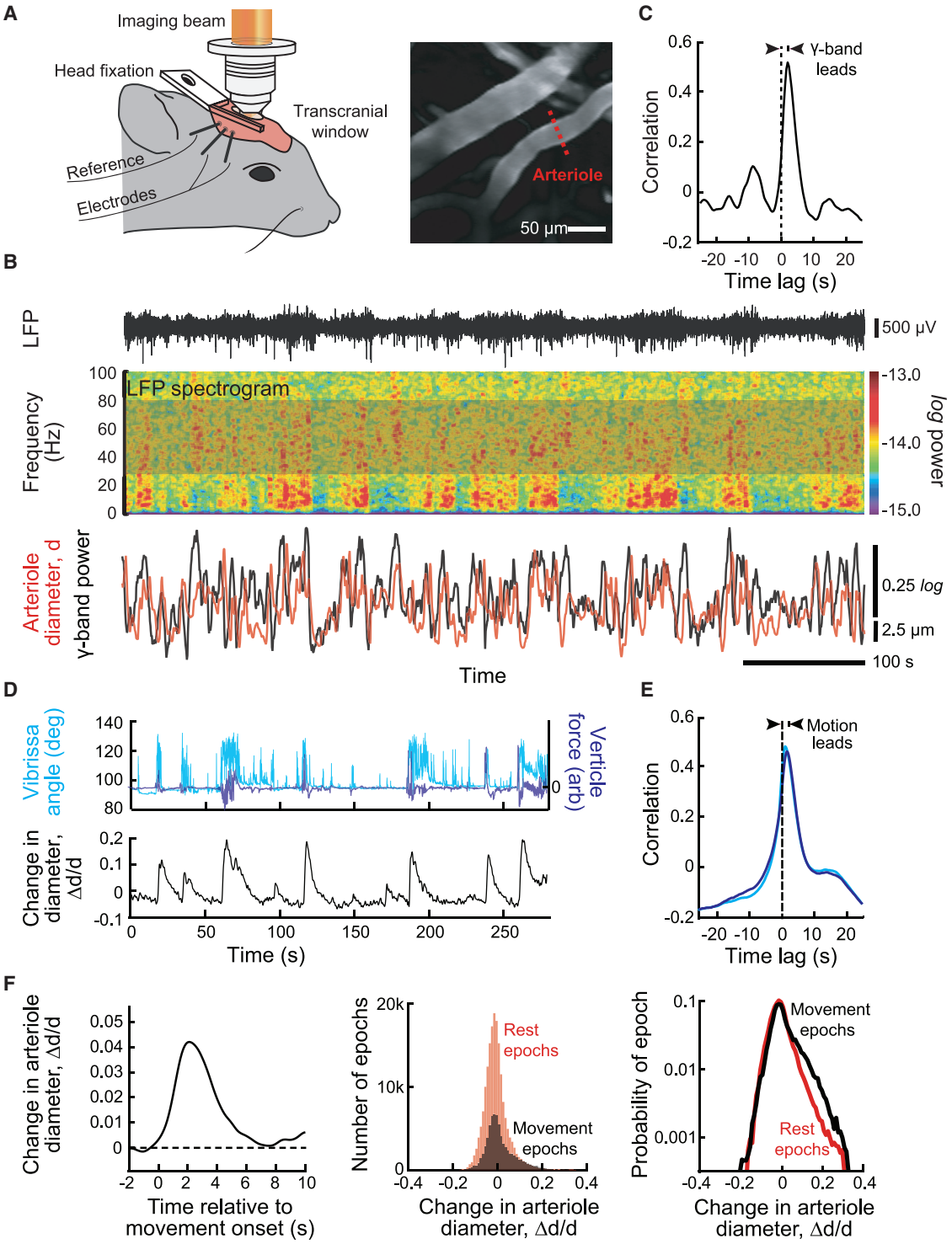

Figure 6. The Envelope of Neuronal γ-Band Oscillations Locks to and Leads Vasomotor Oscillations in Arteriole Diameter

(A) Set-up with a head-fixed awake but resting mouse for two-photon imaging of arteriole diameter along with measurement of the LFP (left panel). A thinned skull window was used to preserve vasomotion (Drew et al., 2010). Shown are two-photon images of surface vessels and the scan path to define lumen diameter (center panel). From Mateo et al. (2017).

(B) Example data showing the LFP (top trace), the spectrogram of the LFP with a window of 2.0 s and a bandwidth of 2.5 Hz, and the time series of the integrated γ-band power and diameter for one arteriole in the field (bottom traces). From Mateo et al. (2017).

(legend continued on next page)

on the short, 2-mm correlation length scale seen in rodents (He et al., 2018; Mateo et al., 2017), nor is there published evidence of even broad-band oscillations at the ~0.1-Hz range. Although we cannot dismiss neuromodulation as a candidate mechanism for locking vasomotion to neuronal activity, current evidence deems it untenable.

ULTRA-SLOW VARIATIONS IN γ-BAND POWER ENTRAIN VASOMOTION

The ability to measure electrophysiological quantities concurrent with vasodynamics is essential to decipher the biophysical basis of resting-state BOLD fMRI signals (Steinbrink et al., 2006). A plethora of past work has made progress with use of mixed electrically and optically based recordings of neuronal activity concurrent with measures of blood flow, often both hemodynamics and vasodynamics, in monkeys (Goense et al., 2012; Goense and Logothetis, 2008; Logothetis et al., 2001, 2012; Schölvinck et al., 2010; Shmuel et al., 2006; Shmuel and Leopold, 2008), rats (Du et al., 2014; He et al., 2018; Schwalm et al., 2017; Thompson et al., 2014), and mice (Anenberg et al., 2014; Lee et al., 2010; Ma et al., 2016; Mateo et al., 2017; Pan et al., 2015; Schulz et al., 2012; Vanni et al., 2017; Wang et al., 2018; Winder et al., 2017). Although mice have the great advantage of genetic introduction of functional labels, this can also lead to complications when insertion of transgenes disrupts the coding sequence of endogenous genes (Goodwin et al., 2019) or labels lead to seizure activity (Steinmetz et al., 2017).

The connection between vasomotor oscillations in pial arterioles and fluctuations in the envelope of the γ-band of the local field potential (LFP) from the superficial layers was established in mice (Mateo et al., 2017). We first consider the temporal variation in the spectral power of the LFP in the upper layers of the cortex in relation to changes in the diameter of surface arterioles (Figure 6A). The field potential shows epochs of enhanced activity across all frequency bands. The variations in power are greatest in the γ-band and, although episodic, are broadly distributed with a periodicity near 0.1 Hz. Crucially, changes in the diameter of surface arterioles co-vary with the power in the γ-band (Figure 6B). The timing of the fluctuations is such that the electrical activity leads that of the diameter by ~2 s in this example (Figure 6C) and as an average over all observations. These data are consistent with the hypothesis that ultra-slow fluctuations in electrical activity drive changes in arteriole diameter. Although the latency between increases in neuronal activity and vasodilation is ~2 s, that between the increase in neural activity and the BOLD fMRI signal is slightly longer, ~3 s, as a result of a delay of the increased oxygenated blood reaching the veins (Mateo et al., 2017; Figure 1A).

To test whether local neuronal activity is sufficient to entrain vasomotion, the neuronal activity in mice that expressed channelrhodopsin in layer 5b pyramidal neurons was driven by light whose intensity was modulated by a 40-Hz γ-rhythm carrier frequency and a 0.1-Hz ultra-slow rhythmic envelope (Mateo et al., 2017). We observed that the envelope of the γ-band and the diameter of a nearby arteriole were phase locked, with electrical activity leading vasodilation by the same ~2 s as observed under natural conditions (Figure 6C). These data confirm that ultra-slow modulation of high-frequency neuronal activity can entrain vasomotion.

The possibility that variations in arteriole diameter drive electrical activity was addressed through use of mice that express halorhodopsin in arteriole smooth muscle (Mateo et al., 2017). Illumination of an arteriole with activating laser light leads to an ~0.2 times dilation, similar to the value seen during vasomotion (Drew et al., 2011). Crucially, driving dilation of the smooth muscle fails to lead to a change in LFP and a large drop in the spectral coherence between the vessel diameter and the driven envelope of the electrical activity. These data support the interpretation that vasomotion does not drive aggregate neuronal activity.

Although the interaction between neuronal activity and vasomotion was unidirectional, an *in vitro* study has demonstrated feedback from blood vessels onto neuronal output (Kim et al., 2016b). Following pressurization of parenchymal arterioles, the vessels develop a myogenic tone. A shift in the level of tone by challenging the arterioles with a change to higher pressure increases constriction, whereas lower pressures led to dilation. Importantly, upon an increase in pressure to induce vasoconstriction, pyramidal neurons suppressed their activity, whereas pressure-evoked dilation led to an increase in pyramidal neuron activity. The relation of this homeostatic feedback mechanism to neurovascular coupling remains an open issue.

"Fidgeting" Movements Are Drivers of Ultra-slow Signals

A potential contributor to the ultra-slow fluctuations in γ-band power are small motor movements of the face and limbs, referred to as fidgeting (Drew et al., 2019; Winder et al., 2017). Studies with humans and primates have shown that blinking (Bristow et al., 2005; Guipponi et al., 2015), swallowing (Birn et al., 1999; Hamdy et al., 1999), and small head motions (Yan

(C) The cross-correlation of the two time series used for the example in (B), 600 s total time, shows that the LFP leads the diameter change. As an average across animals, movement precedes vasodilation by 1.9 ± 0.2 s (82 vessels from 27 mice with 600 s of data per vessel). From Mateo et al. (2017).
(D) New data on the recording of self-generated (i.e., spontaneous) movement in a head-fixed awake but resting mouse, obtained concurrently with two-photon imaging of arteriole diameter (Winder et al., 2017), similar to that in (A), to determine the possible contribution of such movement to the entrainment of vasomotion. Bouts of whisking were determined with videography, and whole-body vertical acceleration was determined with a force sensor attached to the tube supporting the mouse's body.
(E) Correlation analysis of new data (27 vessels from 9 mice with 1,700–12,000 s of data per vessel). The lag-time of the correlation shows that movement leads the change in diameter (bottom panel) with lag times similar to that for movement proceeds the vasodilation by 1.8 ± 0.3 s for whisking and 1.5 ± 0.3 s for whole-body motion.
(F) A re-analysis of the data of Mateo et al. (2017), similar to that for the new data in (E) and this panel, using previously unpublished simultaneous measurements of whole-body horizontal acceleration acquired during imaging (82 vessels from 27 mice). Acceleration leads to a change in arteriole diameter (left panel); the threshold detectability was ~0.01 *g*. Theses movement-related changes in diameter are compared with rest events (center panel) and dominate the largest changes in diameter (right panel).

Please cite this article in press as: Drew et al., Ultra-slow Oscillations in fMRI and Resting-State Connectivity: Neuronal and Vascular Contributions and Technical Confounds, Neuron (2020), https://doi.org/10.1016/j.neuron.2020.07.020

et al., 2013) are accompanied by bilateral activation of motor and somatosensory areas of the brain. Fidgeting appear to be independent of external sensation and, rather, is a consequence of nonvolitional neuronal events. Fidgeting occurs at the rate of several events per minute, enabling these events to drive ultra-slow signals (Huo et al., 2014; Kaminer et al., 2011; Lear et al., 1965). Fidgeting can take place in the absence of stimulation (Stringer et al., 2019) or accompany a learned task in mice (Musall et al., 2019; Salkoff et al., 2019), even though it is irrelevant to the task per se. For example, pressing a bar is accompanied by movements of the face and forelimbs and protraction of the vibrissae. Of relevance to blood flow, the functional form of the coupling between neuronal activity and hemodynamic signals appears to be the same for dilations evoked by fidgeting, sensory stimuli, or volition (Power et al., 2012; Winder et al., 2017; Figures 6D and 6F).

Fidgeting is activated by neuronal motor circuits and presumably drives reafferent or efferent inputs to somatosensory regions in the cortex. Thus, in principle, fidgeting can drive vasodilation and entrain vasomotion. We obtained new data to characterize the relation of fidgeting to entrainment of vasomotion in alert, head-fixed, wild-type mice. Following past methods (Winder et al., 2017), we recorded vibrissa movement, body movement, and concurrent changes in the diameter of pial arterioles (Figure 6D, see experimental details in the legend). Epochs of spontaneous whisking and body motion were observed, the largest of which were clearly correlated with relatively large, transient vasodilation events. As an average over mice and vessels, we observed that the movement preceded vasodilation by ~2 s for whisking and whole-body motion (Figure 6E), similar to that for γ-band power (Figure 6C). Thus, fidgeting is a likely contributor to the source of ultra-slow neuronal activity, but this shifts the question to what neuronal or environmental source drives fidgeting.

We performed a quantitative assessment of the contribution of body movement to the neuronal entrainment of vasomotion across our existing data with head-fixed mice (Mateo et al., 2017; Figures 6A–6C). Previously unpublished accelerometer records of the motion of the body of the mouse were used to determine the contribution of fidgeting to vasomotion (Figure 6F, see experimental details in the legend). As an average over mice and vessels, body motion leads to transient dilation of the pial arterioles that rises over an interval of 2 s, the same as for stimulus-driven changes in arteriole diameter (Figure 1A). The movement-related changes in diameter encompassed 0.27 of the significantly correlated changes between vessel diameter and the γ-band LFP (Figure 6F, center). Critically, fidgeting was correlated with the largest dilations (Figure 6F, right). *In toto*, fidgeting is a significant contributor to the neurological events that entrain vasomotion in mice.

We suggest that fidgeting is likely to play a role in the origin of human resting-state BOLD fMRI signals as well (Drew et al., 2019). The punctate nature of fidgeting events is consistent with the punctate but loosely rhythmic nature of resting-state activity in humans (Liu et al., 2018; Liu and Duyn, 2013; Petridou et al., 2013), and fidgeting behaviors often involve bilateral actions (Drew et al., 2019), consistent with the bilateral nature of spontaneous activations (Figure 2D). Fidgeting behaviors are likely to be associated with BOLD fMRI signals in regions outside of sensory and motor areas of the brain, including areas activated by cognitive tasks. For example, swallowing activates the insula (Martin et al., 2001), and licking (Nakano et al., 2013) and head motion (Bright and Murphy, 2015) activate multiple brain regions. It is an open issue whether the sensorimotor processing associated with fine-scale self-motion is part of the ideation captured by resting-state BOLD fMRI. Nonetheless, experimental designs exist that can flag and censor epochs of even modest self-motion in human subjects (Power et al., 2012; Siegel et al., 2014).

Transitions among Behavioral States May Drive Ultra-slow Signals

A seemingly high proportion of the resting-state BOLD fMRI studies in animals and humans did not closely monitor behavior or arousal. Thus, a wide variety of behavioral states may be sampled and averaged together. Head-fixed mice sleep with their eyes open (Yüzgeç et al., 2018), so careful physiological monitoring of body motion, pupil motion, and pupil size is needed to ensure that the sleep-state vasodynamics (Fultz et al., 2019; Horovitz et al., 2008) do not contaminate resting-state measurements. Post hoc examination of human connectome data has indicated that many subjects, if not most, fall asleep during the scanning process (Tagliazucchi and Laufs, 2014). Sleep-to-wake transitions (Horovitz et al., 2008; Liu et al., 2018) may thus drive events that account for a substantial component of functional connectivity (Liu and Duyn, 2013; Petridou et al., 2013).

MECHANISMS OF CORRELATED BILATERAL VASODYNAMICS

The dominant feature of resting-state connectivity is the bilateral symmetry across hemispheres (Figure 2D). The details of bilateral coactivation can be explored via the coherence between changes in arteriole diameter for vessels in mirrored regions. In fact, precise simultaneous measurements of vessel diameter show that arterioles in mirrored regions oscillate in synchrony with near-unity coherence (Mateo et al., 2017; Figure 3C). The coherence is severely reduced in acallosal mice (Mateo et al., 2017), consistent with the finding that bilateral neuronal signaling is similarly reduced in acallosal mice (Mohajerani et al., 2010). However, as noted previously, the evidence of mirrored activation in acallosal human subjects is equivocal.

Vascular Geometry that Enhances Bilateral Symmetry

Although the origin of symmetry in resting-state connectivity is typically attributed to interhemispheric projections, there are other systemic vascular contributors. Fluctuations in the inflow of blood at the level of the left and right carotids are strongly coherent at 0.01–0.3 Hz, within the range of vasomotor frequencies in awake rats (Revel et al., 2012). Arterial blood oxygenation also fluctuates with fluctuations in respiration rate and with the respiratory cycle (Zhang et al., 2019). These lead to delayed fluctuations in the global BOLD fMRI signal throughout the brain and into the sagittal sinus (Tong et al., 2019). Unfortunately, the fluctuations from the carotid supply tend to dephase as blood travels through the brain with different transit times. Thus,

Please cite this article in press as: Drew et al., Ultra-slow Oscillations in fMRI and Resting-State Connectivity: Neuronal and Vascular Contributions and Technical Confounds, Neuron (2020), https://doi.org/10.1016/j.neuron.2020.07.020

fluctuations in inflow and oxygenation cannot be completely removed by regression of a brain-wide signal (Tong et al., 2015). A further complication occurs because vasomotion changes the transit times. Thus, measures of blood oxygenation can be systematically biased when they occur at locations with different transit times as opposed to mirrored brain regions. For this reason, recent reports of small shifts in the timing of BOLD fMRI signals in humans (Mitra et al., 2015) could be the result of small changes in the perfusion times or oxygenation of blood to different regions of the brain. As a clinical matter, this effect can highlight perfusion deficits after stroke (Lv et al., 2013) and may explain how low-grade brain tumors show coherent oscillations in the BOLD fMRI with their putatively healthy contralateral brain regions (Gupta et al., 2018).

Bilaterally Synchronized Modulatory Inputs Can Drive Bilateral Oscillations

There are direct cholinergic cross-hemispheric connections between the basal forebrain in the two hemispheres (Carnes et al., 1990; Semba et al., 1988). These connections should not be affected in acallosal animals, preserving common input to mirrored, transhemispheric cortical regions.

Activation of the rostral ventral lateral medulla (RVLM), a brain stem nucleus that sits on the ventral surface of the brain below the breathing center (Golanov et al., 1994), leads to an increase in cortical blood flow. This nucleus receives input from neighboring breathing centers (Dempsey et al., 2017) and increases blood flow in response to a decrease in the partial pressure of atmospheric oxygen (pO_2) (Golanov and Reis, 1996). The RVLM contains primarily noradrenergic neurons (Abbott et al., 2012). The limited anatomical studies published to date have not identified direct or complete indirect projections from the RVLM to the cortex (Card et al., 2006). Nonetheless, in one likely pathway, the RVLM projects to the medullary cerebral vasodilator area in the brain stem, then projects to the subthalamic cerebral vasodilator area in the diencephalon, which incorporates the *zona incerta* and the fields of Forel, and finally projects to deep layers of the cortex (Golanov et al., 2001; Ilch and Golanov, 2004). The specifics of the drive to cortical blood vessels is an open issue.

TECHNICAL SOURCES OF ULTRA-SLOW NOISE CONTRIBUTIONS IN fMRI

As a means to reduce voluntary motion of the head, contemporary rodent resting-state fMRI studies have been primarily performed on anesthetized head-fixed but free-breathing animals (Biswal and Kannurpatti, 2009; Williams et al., 2010; Zhao et al., 2008). However, cardiac and respiratory artifacts in rodent resting-state BOLD and CBV fMRI remain to be carefully identified and removed from the data. These difficulties stand in contrast to the significant efforts made for human BOLD fMRI studies (Birn et al., 2006; Dagli et al., 1999; Glover et al., 2000; Hu et al., 1995; Shmueli et al., 2007; Wise et al., 2004). The adoption of signal processing methods developed for human studies (Caballero-Gaudes and Reynolds, 2017; Murphy et al., 2013) will be crucial to reduce the interference of cardiorespiratory artifacts with the spatiotemporal patterns of the resting-state fMRI signals in animals (Abreu et al., 2017; Biswal et al., 1996; Bright and Murphy, 2017; Feinberg and Setsompop, 2013; Kiviniemi et al., 2005).

Respiration-Induced "B_0 Offset" Motion

MRI acquisition relies on Larmor frequency-based spatial encoding through the sequence-specific magnetic field gradients across a subject. The homogeneity of the constant magnetic field, designated B_0, determines the quality of magnetic resonance images (Durand et al., 2001). However, the subject in the magnetic resonance scanner can continually disturb the homogeneity of the B_0 field by body movement (Biswal et al., 1996; Frank et al., 2001; Lowe et al., 1998; Van de Moortele et al., 2002). This includes fidgeting (Figure 6D) as well as breathing and other physiological motions. In practice, breathing leads to an expanding and contracting B_0 field near the brain (Figure 7A). Thus, artifacts in BOLD MRI can originate from parts of the body that are far away from the field of view in the brain (Figure 7B).

Methods to compensate for the time-dependent B_0 field distortions are known (Raj et al., 2000; van Gelderen et al., 2007). However, in contrast to studies on human subjects, the higher magnetic fields used for animal BOLD and CBV fMRI studies exaggerate the effects of physiological contributions to an inhomogeneous B_0 field. In addition, arteriole CO_2 (Wise et al., 2004) and respiratory volume changes (Birn et al., 2006) can cause variations in the resting-state BOLD fMRI signals that lead to falsely interpreted signals.

Aliasing of Physiological Rhythms

Rats have an approximately 5- to 7-Hz cardiac frequency and approximately 1- to 2-Hz respiration rates under anesthesia. The conventional echo-planar imaging protocol with rodents involves a 1- to 2-s period of repetition (RT) or, equivalently, a sampling rate, f_s, of 1/RT = 0.5–1.0 Hz. The low rate of sampling compared with physiological processes that distort the fMRI signal causes aliasing of cardiac and respiratory contributions down to frequencies that may also be erroneously associated with resting-state dynamics. This is well described for human resting-state fMRI studies (Biswal et al., 1996; Dagli et al., 1999; De Luca et al., 2006; Frank et al., 2001; Lowe et al., 1998) and is seen in rats as well (Pais-Roldán et al., 2018). For example, when f_s = 0.8 Hz and the spontaneous breathing rate (f_B) of an anesthetized rat is 1.0 ± 0.1 Hz, the signal is aliased to $f_B - f_s = 0.2 \pm 0.1$ Hz. This is illustrated by measuring breathing at $f_s >> f_B$ and observing the aliased rate that is seen when the data are down-sampled to f_s = 0.8 Hz (Figure 7C). Aliasing is observed in the fMRI signal of the brain and a phantom above the head of the animal when f_s = 0.8 Hz (Figure 7C). This illustrates the combined effect of distortion of the B_0 field and aliasing to form a false image of a resting-sate signal (Figure 7D).

Fast fMRI methods clearly avoid aliasing of the cardiac and respiratory contributions to the fMRI signals from rodents (Williams et al., 2010; Yu et al., 2014). A similar fast sampling strategy has been well implemented to remove the physiological noise of fMRI measurements from human brains (Agrawal et al., 2020). However, it is much more difficult to avoid the higher-frequency cardiac-specific aliasing artifacts, especially for awake rodent fMRI (Desai et al., 2011; Ferenczi et al., 2016; Liang et al., 2015). Further, cardiac and respiratory cycles can fluctuate

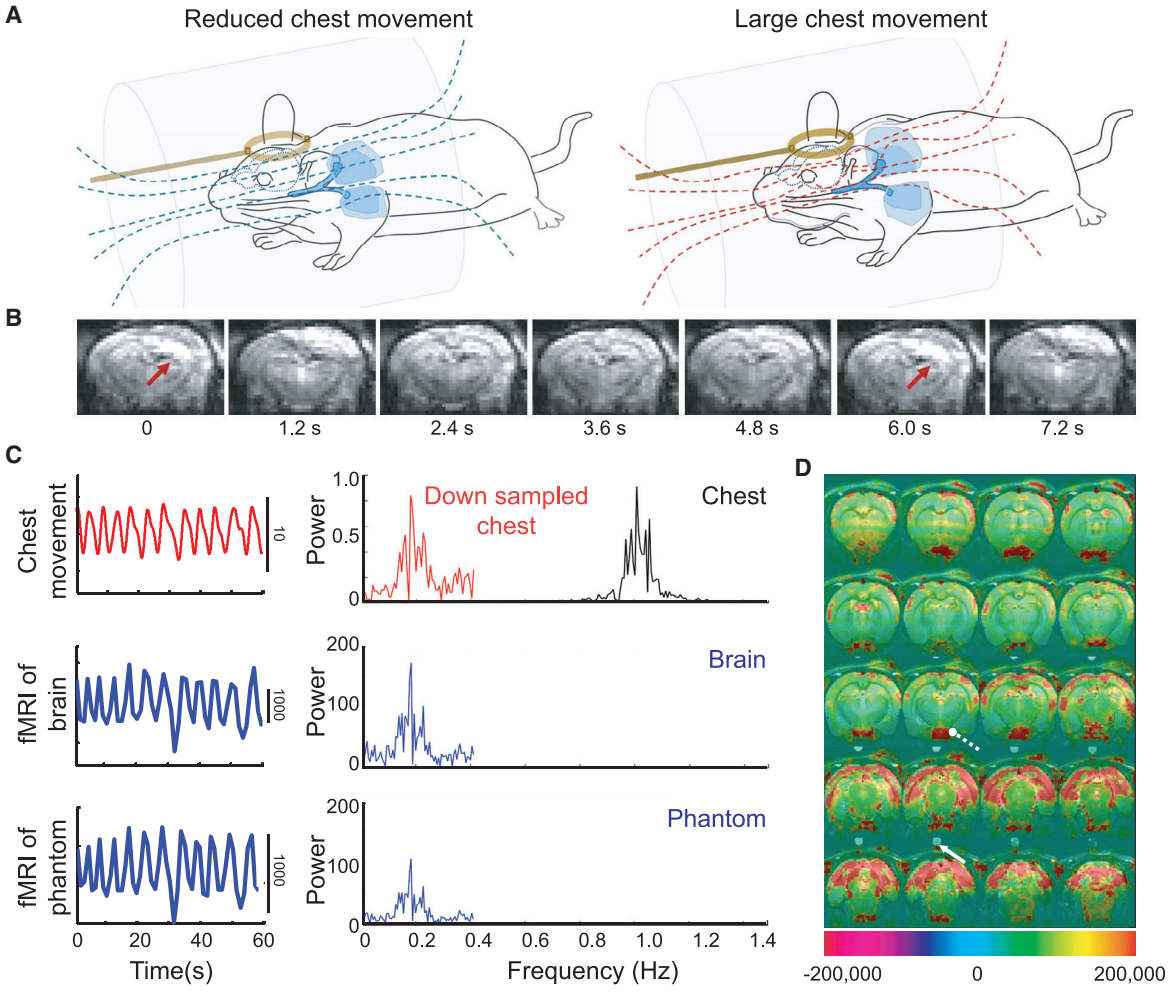

Figure 7. The Aliasing Effect of Respiration-Induced Magnetic Field (B_0) Distortion

(A) Schematic drawing of the B_0 field on free-breathing rats with different extents of chest movements and associated magnetic field lines. The distorted B_0 field is caused by the large chest movement during the respiratory cycles (red lines). Amber circles are pickup coils. From Pais-Roldán et al. (2018).

(B) Coronal sections from a three-dimensional echo-planar imaging sequence acquired at 1.2-s repetition time (RT), from 0 to 7.2 s, from a spontaneously breathing anesthetized rat. These data show the effect of the B_0-related motion artifacts at ~0.16 Hz as a function of time. From Pais-Roldán et al. (2018).

(C) The respiratory trace (black, chest movement) and the down-sampled time course (red line) for a 1/RT sampling rate with RT = 1.2 s (top panel). The power spectral density shows the aliased signal, peaked ($f_{res} - 1/RT$) (i.e., 0.16 Hz), of which the f_{res} is around 1.0 ± 0.1 Hz. The fMRI time course and spectral density of a voxel in the brain (center panel) or in a phantom (bottom panel) over the animal's head shows the oscillatory signal with a bandwidth of 0.16 ± 0.1 Hz, which is dominated by the respiration-induced B_0 artifacts. The brain and phantom voxels are defined by the two arrows in (D). From Pais-Roldán et al. (2018).

(D) Map of the power at the artifact frequency, 0.16 ± 0.1 Hz, showing the voxel-wise spatial correlation to the B_0-related artifacts. The high-power scales indicate the strong B_0-related artifacts. From Pais-Roldán et al. (2018).

individually and in a coupled manner at frequencies close to the ~0.1-Hz frequency range for ultra-slow signals. These fluctuations can serve as additional, confounding sources for resting-state BOLD fMRI studies (Shmueli et al., 2007).

CONCLUSIONS

Motivated by a desire to understand the biophysical basis of resting-state fMRI (Figure 2), we reviewed data on the relation of spontaneous changes in blood flow and blood oxygenation in the brain to changes in the underlying neuronal activity (Figure 8A). Ultra-slow vasomotor oscillations occur in the smooth muscle cells that encircle brain arterioles and lead to rhythmic changes in the diameter of arterioles within a frequency band near 0.1 Hz (Figure 3). Further, collective neuronal dynamics in the forebrain lead to generation of high-frequency γ-band oscillations whose amplitude is modulated at the ultra-slow rate of ~0.1 Hz (Figure 6B). These ultra-slow neuronal oscillations entrain arteriole oscillations to link brain vasodynamics with non-volitional neuronal activity (Figures 6A–6C). The entrainment is statistically significant (Figure 6) even though the vasculature also responds to common, cortex-wide inputs and homeostatic physiological inputs. Entrainment of vasomotion by neuronal spiking provides a means for arterioles in regions of the brain that are separated but connected through callosal projections to have synchronous vasomotor activity (Figure 3C). Within the technological

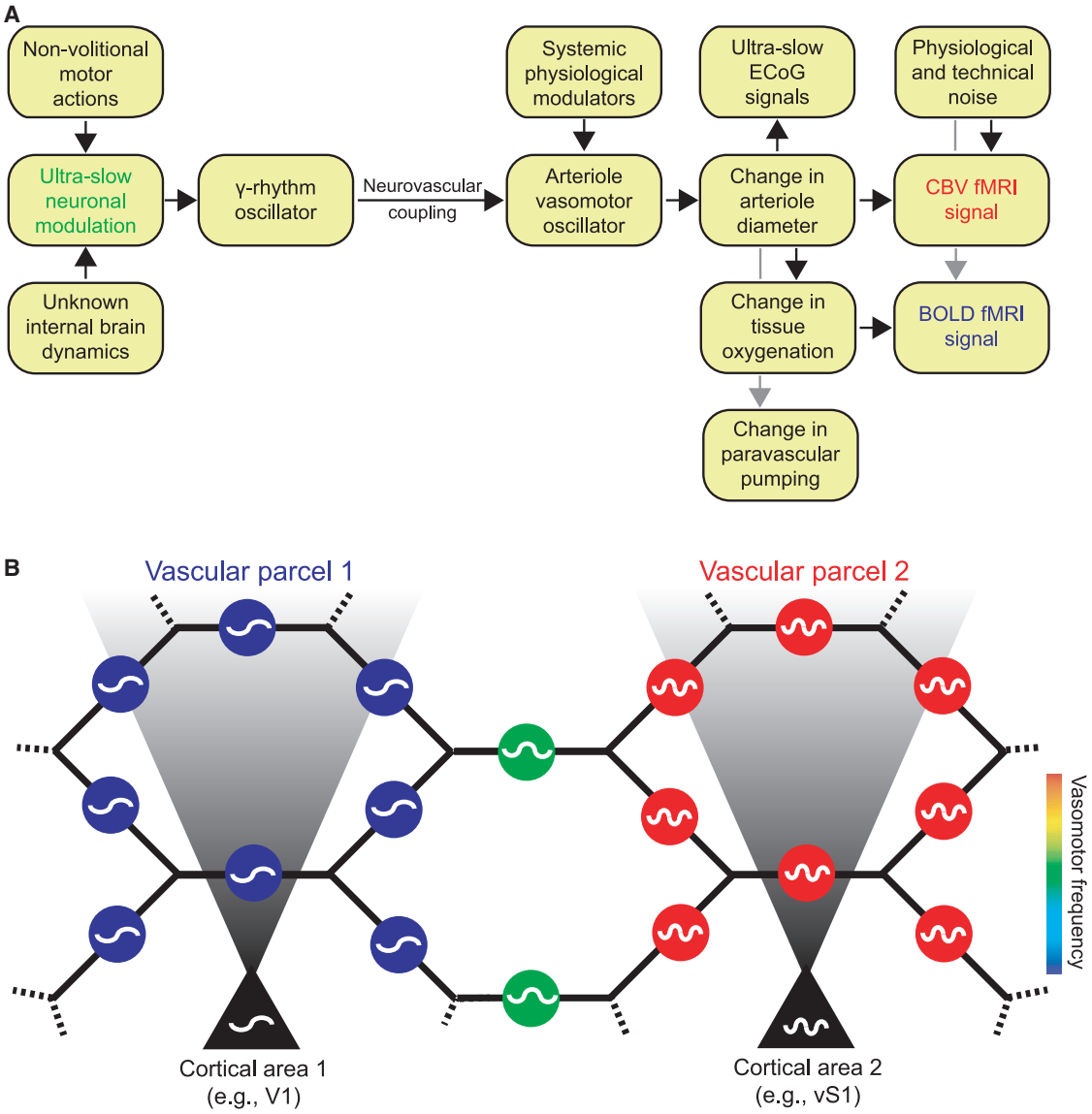

Figure 8. Coupled Oscillator Model for Resting-State Neurovascular Coupling

(A) Interactions for one region. Variations in γ-band electrical power lead to partial entrainment of the vasomotor oscillations in the smooth muscle of cortical surface and penetrating arterioles. Increases in γ-band electrical power dilate the arterioles and lead to an increase in the supply of fresh blood, as measured by CBV fMRI. The increase in diameter subsequently leads to an increase in blood oxygenation and a positive change in the BOLD fMRI signal. Coupling can be via callosal projections or via common input.

(B) Circuit of the pial arteriole network in terms of coupled smooth muscle oscillators. Each oscillator represents the activity of all muscles in one arteriole. The oscillators communicate with one another via the hexagonal lattice of electrically joined endothelial cells that form the lumen (Figure 6). Oscillators in a given region of the brain may also receive electrical input from underlying neuronal oscillators. This input can dominate and lead to parcellation of the frequency of vasomotor oscillations, as observed by fMRI (Figure 2B). Vasomotion is synchronous within a given region of the brain but can occur with different frequencies in different regions (labeled blue and red for regions 1 and 2, respectively, and labeled green for an intermediate region without neuronal drive).

framework of fMRI, vasomotor activity can be measured through changes in arteriole volume (CBV fMRI) or changes in blood oxygenation secondary to changes in diameter (BOLD fMRI). The flow diagram in Figure 8A formalizes this description.

Significance of Ultra-slow Coupling

Functional MRI allows one to "decode" the neural activity in the brain to the extent that neural activity is represented by BOLD signals (Kay et al., 2008). A key issue is how well hemodynamic signals report neural activity. In Table S1, we list the correlation coefficient R^2, the so-called "variance explained," between neural activity and the BOLD or CBV fMRI or equivalent optical signal; Box S1 relates R^2 to the spectral coherence, $C(f)$. In all of these studies, there was a highly significant correlation between the hemodynamic response and neural activity. This means that the resting-state BOLD fMRI signal or equivalents

Please cite this article in press as: Drew et al., Ultra-slow Oscillations in fMRI and Resting-State Connectivity: Neuronal and Vascular Contributions and Technical Confounds, Neuron (2020), https://doi.org/10.1016/j.neuron.2020.07.020

are, to varying extents, driven by neural activity. However, the value of R^2 is universally less than 0.5 and typically around 0.1 (Schölvinck et al., 2010; Shmuel and Leopold, 2008). This means that only 0.1–0.5 of the hemodynamic signal is related to neural activity. An R^2 value of 0.5 between γ-band neuronal activity and the simultaneously recorded BOLD fMRI signal occurs for visual stimulus-evoked activity in the un-anesthetized primate (Goense and Logothetis, 2008). Given the strong drive of visual stimuli, this suggest that the R^2 value of 0.5 seen in resting-state measurement is likely to be an upper bound. If we further consider that fidgeting occurs ~0.3 of the time, then, as an upper bound, we expect that, at most, 0.5 × 0.7 ~0.4 of the resting-state BOLD fMRI signal is related to internally driven brain dynamics. Thus, resting-state BOLD fMRI, as currently practiced, provides unique capabilities to infer connectivity in the human brain but is a technique with an inherently low signal-to-noise ratio.

The Role of Vasomotion

What is the normal physiological purpose served by the ultra-slow vasomotor oscillations of brain arterioles? Recent work points to the necessity of vasomotion for clearance of large solutes (van Veluw et al., 2020), principally through the paravascular space between smooth muscle and endothelial cells (Cserr and Ostrach, 1974; Rennels et al., 1985). These solutes include β-amyloid (Iliff et al., 2012). To the extent that vasomotion is entrained by the envelope of the γ-band power (Mateo et al., 2017; Figure 6), it is of interest whether increases in γ-power in the brain through sensory stimulation also increase clearance of β-amyloid (Iaccarino et al., 2016). The ability of vasomotion to drive solutes must depend on a mechanism to set the direction of flow, such as peristaltic motion (Aldea et al., 2019) or still unknown valves in the paravascular space (Mathiisen et al., 2010).

Next Steps

The nature of the local neuronal circuitry that generates ultra-slow signals and modulates the γ-rhythm remains an open issue. In particular, the exact frequency of ultra-slow signals varies across the brain with millimeters to centimeters of coherence (Mitra et al., 1997; Vanni et al., 2017; Figure 2B). Such spatially restricted modulation could be accomplished by even small changes in activation of currents in individual cells that contribute to generate the γ-rhythm (Kopell and LeMasson, 1994). In this way, the ultra-slow signals are purely modulatory (Figure 4), and the ECoG will not contain ultra-slow signals (Figure 5).

Recent work describes a fast mechanism to transform subsurface microvasculature signaling into changes in arteriole diameter (Longden et al., 2017; Figure 1C). However, the nature of electrical signaling across the network of pial surface vasculature remains to be solved (Hillman, 2014). At a phenomenological level, the pial arteriole oscillators form two sets of interactions (Figure 8B). On one hand, each arteriole is directly connected to four neighboring oscillators (Blinder et al., 2010) via gap junctions between endothelial cells (Figure 1C); this connectivity will act to frequency-lock vasomotion across all vessels across the surface (Sakaguchi et al., 1988; Strogatz and Mirolla, 1988). On the other hand, underlying neurons can drive the local pial vessels at different frequencies; this should break the coherence of vessels across the cortical mantle so that the vessels parcellate into regions with different vasomotor center frequencies (Figure 8B). BOLD fMRI data from humans support such a parcellation on a scale of tens of millimeters (Figure 1B). In fact, such parcellation has been used to segment different regions in the cortex (Fox et al., 2005; Glasser et al., 2016). Animal models together with large-field, high-precision optical imaging (Sofroniew et al., 2016; Tsai et al., 2015) should allow us to assess the phenomenology and the biophysics of this parcellation.

A more accurate and high-resolution measure of functional connectivity may be obtained through measurements of CBV rather than BOLD fMRI (He et al., 2018). When the spatial resolution of fMRI can distinguish individual vessels that penetrate the cortex of the rat brain (Moon et al., 2013; Poplawsky et al., 2019; Yu et al., 2012), the BOLD fMRI signal is located mainly at venule voxels, whereas the CBV fMRI signal is detected primarily at arteriole voxels (He et al., 2018; Yu et al., 2016). Thus, the single-vessel fMRI method enables detection of the spatial correlation patterns of the resting-state signal with vascular specificity, as seen optically in restricted regions (Mateo et al., 2017; Figure 3C). From a technical perspective, the spatial localization of single-vessel fMRI decouples the resting-state signal from respiration-induced B_0-related motion artifacts (Figure 7). The ability to resolve individual penetrating vessels with CBV fMRI provides a critical platform to explore the ultra-slow oscillatory patterns of vasodynamics across the brain. This is particularly important for understanding how pairwise interactions among different brain regions may lead to the multitude of default networks of rodent (Chan et al., 2015; Ma et al., 2016; Mohajerani et al., 2010, 2013) and human (Greicius et al., 2003; Raichle et al., 2001; Sporns et al., 2005) brain activity.

Finally, as a practical matter, experimenters should monitor behavior and arousal state as much as possible to differentiate between activity generated during spontaneous movements, sleep, and activity generated during true "rest" (Drew et al., 2019). Monitoring of the behavioral state has become de rigueur in systems neuroscience experiments using awake rodents and primates (Egnor and Branson, 2016; Whishaw and Whishaw, 2014), makes use of standard equipment for studies with rodents (Kurnikova et al., 2017; Mathis et al., 2018; Reimer et al., 2014), and should be adopted by the human fMRI community as well. Thus, it may be possible to use behavioral event markers to segregate resting-state epochs with fidgeting from those without these movements and, presumably, increase the sensitivity to purely intrinsically driven brain-wide changes in BOLD or CBV fMRI signals.

SUPPLEMENTAL INFORMATION

Supplemental Information can be found online at https://doi.org/10.1016/j.neuron.2020.07.020.

ACKNOWLEDGMENTS

We thank David Boas, Thomas Broggini, Jean-Pierre Changeux, Karishma Chhabria, Anna Devor, Jessica Filosa, Partha Mitra, Mark Nelson, Jonathan Polimeni, Bruce Rosen, Kamil Urgurbil, and Massimo Vergassola for valuable discussions. We thank Beth Friedman for critical comments on drafts of this

manuscript. This work was supported by grants EB0217003, MH114224, and NS078168 (to P.J.D.); MH111438 and NS097265 (to D.K.); and NS113278 (to X.Y.) and the Max Planck Society.

REFERENCES

Aalkjaer, C., and Nilsson, H. (2005). Vasomotion: cellular background for the oscillator and for the synchronization of smooth muscle cells. Br. J. Pharmacol. *144*, 605–616.

Aalkjær, C., Boedtkjer, D., and Matchkov, V. (2011). Vasomotion - what is currently thought? Acta Physiol. (Oxf.) *202*, 253–269.

Abbott, S.B., Kanbar, R., Bochorishvili, G., Coates, M.B., Stornetta, R.L., and Guyenet, P.G. (2012). C1 neurons excite locus coeruleus and A5 noradrenergic neurons along with sympathetic outflow in rats. J. Physiol. *590*, 2897–2915.

Abreu, R., Nunes, S., Leal, A., and Figueiredo, P. (2017). Physiological noise correction using ECG-derived respiratory signals for enhanced mapping of spontaneous neuronal activity with simultaneous EEG-fMRI. Neuroimage *154*, 115–127.

Adachi, T., Baramidze, D.G., and Sato, A. (1992). Stimulation of the nucleus basalis of Meynert increases cortical cerebral blood flow without influencing diameter of the pial artery in rats. Neurosci. Lett. *143*, 173–176.

Agrawal, U., Brown, E.N., and Lewis, L.D. (2020). Model-based physiological noise removal in fast fMRI. Neuroimage *205*, 116231.

Ahrens, K.F., Levine, H., Suhl, H., and Kleinfeld, D. (2002). Spectral mixing of rhythmic neuronal signals in sensory cortex. Proc. Natl. Acad. Sci. USA *99*, 15176–15181.

Aldea, R., Weller, R.O., Wilcock, D.M., Carare, R.O., and Richardson, G. (2019). Cerebrovascular smooth muscle cells as the drivers of intramural periarterial drainage of the brain. Front. Aging Neurosci. *11*, 1.

Anenberg, E., Arstikaitis, P., Niitsu, Y., Harrison, T.C., Boyd, J.D., Hilton, B.J., Tetzlaff, W., and Murphy, T.H. (2014). Ministrokes in channelrhodopsin-2 transgenic mice reveal widespread deficits in motor output despite maintenance of cortical neuronal excitability. J. Neurosci. *34*, 1094–1104.

Attwell, D., Buchan, A.M., Charpak, S., Lauritzen, M., Macvicar, B.A., and Newman, E.A. (2010). Glial and neuronal control of brain blood flow. Nature *468*, 232–243.

Bandettini, P.A., Wong, E.C., Hinks, R.S., Tikofsky, R.S., and Hyde, J.S. (1992). Time course EPI of human brain function during task activation. Magn. Reson. Med. *25*, 390–397.

Barson, D., Hamodi, A.S., Shen, X., Lur, G., Constable, R.T., Cardin, J.A., Crair, M.C., and Higley, M.J. (2020). Simultaneous mesoscopic and two-photon imaging of neuronal activity in cortical circuits. Nat. Methods *17*, 107–113.

Belliveau, J.W., Kennedy, D.N., Jr., McKinstry, R.C., Buchbinder, B.R., Weisskoff, R.M., Cohen, M.S., Vevea, J.M., Brady, T.J., and Rosen, B.R. (1991). Functional mapping of the human visual cortex by magnetic resonance imaging. Science *254*, 716–719.

Besson, J.M., Woody, C.D., Aleonard, P., Thompson, H.K., Albe-Fessard, D., and Marshall, W.H. (1970). Correlations of brain d-c shifts with changes in cerebral blood flow. Am. J. Physiol. *218*, 284–291.

Birn, R.M., Bandettini, P.A., Cox, R.W., and Shaker, R. (1999). Event-related fMRI of tasks involving brief motion. Hum. Brain Mapp. *7*, 106–114.

Birn, R.M., Diamond, J.B., Smith, M.A., and Bandettini, P.A. (2006). Separating respiratory-variation-related fluctuations from neuronal-activity-related fluctuations in fMRI. Neuroimage *31*, 1536–1548.

Biswal, B.B., and Kannurpatti, S.S. (2009). Resting-state functional connectivity in animal models: Modulations by exsanguination. Methods Mol. Biol. *489*, 255–274.

Biswal, B., Yetkin, F.Z., Haughton, V.M., and Hyde, J.S. (1995). Functional connectivity in the motor cortex of resting human brain using echo-planar MRI. Magn. Reson. Med. *34*, 537–541.

Biswal, B., DeYoe, E.A., and Hyde, J.S. (1996). Reduction of physiological fluctuations in fMRI using digital filters. Magn. Reson. Med. *35*, 107–113.

Biswal, B.B., Mennes, M., Zuo, X.-N., Gohel, S., Kelly, C., Smith, S.M., Beckmann, C.F., Adelstein, J.S., Buckner, R.L., Colcombe, S., et al. (2010). Toward discovery science of human brain function. Proc. Natl. Acad. Sci. USA *107*, 4734–4739.

Black, H.S. (1953). Modulation Theory (Van Nostrand).

Blinder, P., Shih, A.Y., Rafie, C., and Kleinfeld, D. (2010). Topological basis for the robust distribution of blood to rodent neocortex. Proc. Natl. Acad. Sci. USA *107*, 12670–12675.

Bohland, J.W., Wu, C., Barbas, H., Bokil, H., Bota, M., Breiter, H.C., Cline, H.T., Doyle, J.C., Freed, P.J., Greenspan, R.J., et al. (2009). A proposal for a coordinated effort for the determination of brainwide neuroanatomical connectivity in model organisms at a mesoscopic scale. PLoS Comput. Biol. *5*, e1000334.

Branscomb, L.M. (1995). Confessions of a Technophile (American Institute of Physics).

Bright, M.G., and Murphy, K. (2015). Is fMRI "noise" really noise? Resting state nuisance regressors remove variance with network structure. Neuroimage *114*, 158–169.

Bright, M.G., and Murphy, K. (2017). Cleaning up the fMRI time series: Mitigating noise with advanced acquisition and correction strategies. Neuroimage *154*, 1–3.

Bristow, D., Frith, C., and Rees, G. (2005). Two distinct neural effects of blinking on human visual processing. Neuroimage *27*, 136–145.

Buxton, R.B. (2001). The elusive initial dip. Neuroimage *13*, 953–958.

Caballero-Gaudes, C., and Reynolds, R.C. (2017). Methods for cleaning the BOLD fMRI signal. Neuroimage *154*, 128–149.

Caesar, K., Akgören, N., Mathiesen, C., and Lauritzen, M. (1999). Modification of activity-dependent increases in cerebellar blood flow by extracellular potassium in anaesthetized rats. J. Physiol. *520*, 281–292.

Card, J.P., Sved, J.C., Craig, B., Raizada, M., Vazquez, J., and Sved, A.F. (2006). Efferent projections of rat rostroventrolateral medulla C1 catecholamine neurons: Implications for the central control of cardiovascular regulation. J. Comp. Neurol. *499*, 840–859.

Cardin, J.A., Carlén, M., Meletis, K., Knoblich, U., Zhang, F., Deisseroth, K., Tsai, L.H., and Moore, C.I. (2009). Driving fast-spiking cells induces gamma rhythm and controls sensory responses. Nature *459*, 663–667.

Cardoso, M.M.B., Lima, B., Sirotin, Y.B., and Das, A. (2019). Task-related hemodynamic responses are modulated by reward and task engagement. PLoS Biol. *17*, e3000080.

Carnes, K.M., Fuller, T.A., and Price, J.L. (1990). Sources of presumptive glutamatergic/aspartatergic afferents to the magnocellular basal forebrain in the rat. J. Comp. Neurol. *302*, 824–852.

Cauli, B., and Hamel, E. (2010). Revisiting the role of neurons in neurovascular coupling. Front. Neuroenergetics *2*, 9.

Chan, A.W., Mohajerani, M.H., LeDue, J.M., Wang, Y.T., and Murphy, T.H. (2015). Mesoscale infraslow spontaneous membrane potential fluctuations recapitulate high-frequency activity cortical motifs. Nat. Commun. *6*, 7738.

Cserr, H.F., and Ostrach, L.H. (1974). Bulk flow of interstitial fluid after intracranial injection of blue dextran 2000. Exp. Neurol. *45*, 50–60.

Dacey, R.G., Jr., and Duling, B.R. (1984). Effect of norepinephrine on penetrating arterioles of rat cerebral cortex. Am. J. Physiol. Heart Circ. Physiol. *246*, 380–385.

Dagli, M.S., Ingeholm, J.E., and Haxby, J.V. (1999). Localization of cardiac-induced signal change in fMRI. Neuroimage *9*, 407–415.

De Luca, M., Smith, S., De Stefano, N., Federico, A., and Matthews, P.M. (2005). Blood oxygenation level dependent contrast resting state networks are relevant to functional activity in the neocortical sensorimotor system. Exp. Brain Res. *167*, 587–594.

De Luca, M., Beckmann, C.F., De Stefano, N., Matthews, P.M., and Smith, S.M. (2006). fMRI resting state networks define distinct modes of long-distance interactions in the human brain. Neuroimage *29*, 1359–1367.

Dempsey, B., Le, S., Turner, A., Bokiniec, P., Ramadas, R., Bjaalie, J.G., Menuet, C., Neve, R., Allen, A.M., Goodchild, A.K., and McMullan, S. (2017). Mapping and analysis of the connectome of sympathetic premotor neurons in the rostral ventrolateral medulla of the rat using a volumetric brain atlas. Front. Neural Circuits *11*, 9.

Desai, M., Kahn, I., Knoblich, U., Bernstein, J., Atallah, H., Yang, A., Kopell, N., Buckner, R.L., Graybiel, A.M., Moore, C.I., and Boyden, E.S. (2011). Mapping brain networks in awake mice using combined optical neural control and fMRI. J. Neurophysiol. *105*, 1393–1405.

Drew, P.J., Duyn, J.H., Golanov, E., and Kleinfeld, D. (2008). Finding coherence in spontaneous oscillations. Nat. Neurosci. *11*, 991–993.

Drew, P.J., Shih, A.Y., Driscoll, J.D., Knutsen, P.M., Blinder, P., Davalos, D., Akassoglou, K., Tsai, P.S., and Kleinfeld, D. (2010). Chronic optical access through a polished and reinforced thinned skull. Nat. Methods *7*, 981–984.

Drew, P.J., Shih, A.Y., and Kleinfeld, D. (2011). Fluctuating and sensory-induced vasodynamics in rodent cortex extend arteriole capacity. Proc. Natl. Acad. Sci. USA *108*, 8473–8478.

Drew, P.J., Winder, A.T., and Zhang, Q. (2019). Twitches, blinks, and fidgets: Important generators of ongoing neural activity. Neuroscientist *25*, 298–313.

Du, C., Volkow, N.D., Koretsky, A.P., and Pan, Y. (2014). Low-frequency calcium oscillations accompany deoxyhemoglobin oscillations in rat somatosensory cortex. Proc. Natl. Acad. Sci. USA *111*, E4677–E4686.

Durand, E., van de Moortele, P.F., Pachot-Clouard, M., and Le Bihan, D. (2001). Artifact due to B(0) fluctuations in fMRI: correction using the k-space central line. Magn. Reson. Med. *46*, 198–201.

Egnor, S.E.R., and Branson, K. (2016). Computational analysis of behavior. Annu. Rev. Neurosci. *39*, 217–236.

Engel, A.K., König, P., Kreiter, A.K., and Singer, W. (1991). Interhemispheric synchronization of oscillatory neuronal responses in cat visual cortex. Science *252*, 1177–1179.

Feinberg, D.A., and Setsompop, K. (2013). Ultra-fast MRI of the human brain with simultaneous multi-slice imaging. J. Magn. Reson. *229*, 90–100.

Ferenczi, E.A., Zalocusky, K.A., Liston, C., Grosenick, L., Warden, M.R., Amatya, D., Katovich, K., Mehta, H., Patenaude, B., Ramakrishnan, C., et al. (2016). Prefrontal cortical regulation of brainwide circuit dynamics and reward-related behavior. Science *351*, aac9698.

Ferezou, I., Haiss, F., Gentet, L.J., Aronoff, R., Weber, B., and Petersen, C.C.H. (2007). Spatiotemporal dynamics of cortical sensorimotor integration in behaving mice. Neuron *56*, 907–923.

Filosa, J.A., Bonev, A.D., Straub, S.V., Meredith, A.L., Wilkerson, M.K., Aldrich, R.W., and Nelson, M.T. (2006). Local potassium signaling couples neuronal activity to vasodilation in the brain. Nat. Neurosci. *9*, 1397–1403.

Fox, P.T., and Lancaster, J.L. (2002). Opinion: Mapping context and content: the BrainMap model. Nat. Rev. Neurosci. *3*, 319–321.

Fox, M.D., and Raichle, M.E. (2007). Spontaneous fluctuations in brain activity observed with functional magnetic resonance imaging. Nat. Rev. Neurosci. *8*, 700–711.

Fox, M.D., Snyder, A.Z., Vincent, J.L., Corbetta, M., Van Essen, D.C., and Raichle, M.E. (2005). The human brain is intrinsically organized into dynamic, anticorrelated functional networks. Proc. Natl. Acad. Sci. USA *102*, 9673–9678.

Frank, L.R., Buxton, R.B., and Wong, E.C. (2001). Estimation of respiration-induced noise fluctuations from undersampled multislice fMRI data. Magn. Reson. Med. *45*, 635–644.

Fultz, N.E., Bonmassar, G., Setsompop, K., Stickgold, R.A., Rosen, B.R., Polimeni, J.R., and Lewis, L.D. (2019). Coupled electrophysiological, hemodynamic, and cerebrospinal fluid oscillations in human sleep. Science *366*, 628–631.

Gao, Y.R., Ma, Y., Zhang, Q., Winder, A.T., Liang, Z., Antinori, L., Drew, P.J., and Zhang, N. (2017). Time to wake up: Studying neurovascular coupling and brain-wide circuit function in the un-anesthetized animal. Neuroimage *153*, 382–398.

Gielow, M.R., and Zaborszky, L. (2017). The input-output relationship of the cholinergic basal forebrain. Cell Rep. *18*, 1817–1830.

Glasser, M.F., Coalson, T.S., Robinson, E.C., Hacker, C.D., Harwell, J., Yacoub, E., Ugurbil, K., Andersson, J., Beckmann, C.F., Jenkinson, M., et al. (2016). A multi-modal parcellation of human cerebral cortex. Nature *536*, 171–178.

Glover, G.H., Li, T.Q., and Ress, D. (2000). Image-based method for retrospective correction of physiological motion effects in fMRI: RETROICOR. Magn. Reson. Med. *44*, 162–167.

Goense, J.B.M., and Logothetis, N.K. (2008). Neurophysiology of the BOLD fMRI signal in awake monkeys. Curr. Biol. *18*, 631–640.

Goense, J., Merkle, H., and Logothetis, N.K. (2012). High-resolution fMRI reveals laminar differences in neurovascular coupling between positive and negative BOLD responses. Neuron *76*, 629–639.

Golanov, E.V., and Reis, D.J. (1996). Contribution of oxygen-sensitive neurons of the rostral ventrolateral medulla to hypoxic cerebral vasodilatation in the rat. J. Physiol. *495*, 201–216.

Golanov, E.V., Yamamoto, S., and Reis, D.J. (1994). Spontaneous waves of cerebral blood flow associated with a pattern of electrocortical activity. Am. J. Physiol. *266*, R204–R214.

Golanov, E.V., Christensen, J.R., and Reis, D.J. (2001). Neurons of a limited subthalamic area mediate elevations in cortical cerebral blood flow evoked by hypoxia and excitation of neurons of the rostral ventrolateral medulla. J. Neurosci. *21*, 4032–4041.

Goodwin, L.O., Splinter, E., Davis, T.L., Urban, R., He, H., Braun, R.E., Chesler, E.J., Kumar, V., van Min, M., Ndukum, J., et al. (2019). Large-scale discovery of mouse transgenic integration sites reveals frequent structural variation and insertional mutagenesis. Genome Res. *29*, 494–505.

Gozzi, A., and Schwarz, A.J. (2016). Large-scale functional connectivity networks in the rodent brain. Neuroimage *127*, 496–509.

Greicius, M.D., Krasnow, B., Reiss, A.L., and Menon, V. (2003). Functional connectivity in the resting brain: a network analysis of the default mode hypothesis. Proc. Natl. Acad. Sci. USA *100*, 253–258.

Greicius, M.D., Supekar, K., Menon, V., and Dougherty, R.F. (2009). Resting-state functional connectivity reflects structural connectivity in the default mode network. Cereb. Cortex *19*, 72–78.

Grinvald, A., Frostig, R.D., Lieke, E., and Hildesheim, R. (1988). Optical imaging of neuronal activity. Physiol. Rev. *68*, 1285–1366.

Grinvald, A., Frostig, R.D., Siegel, R.M., and Bartfeld, E. (1991). High-resolution optical imaging of functional brain architecture in the awake monkey. Proc. Natl. Acad. Sci. USA *88*, 11559–11563.

Guipponi, O., Odouard, S., Pinède, S., Wardak, C., and Ben Hamed, S. (2015). fMRI cortical correlates of spontaneous eye blinks in the nonhuman primate. Cereb. Cortex *25*, 2333–2345.

Gupta, L., Gupta, R.K., Postma, A.A., Sahoo, P., Gupta, P.K., Patir, R., Ahlawat, S., Saha, I., and Backes, W.H. (2018). Advanced and amplified BOLD fluctuations in high-grade gliomas. J. Magn. Reson. Imaging *47*, 1616–1625.

Haddock, R.E., and Hill, C.E. (2005). Rhythmicity in arterial smooth muscle. J. Physiol. *566*, 645–656.

Hamdy, S., Rothwell, J.C., Brooks, D.J., Bailey, D., Aziz, Q., and Thompson, D.G. (1999). Identification of the cerebral loci processing human swallowing with $H_2{}^{(15)}O$ PET activation. J. Neurophysiol. *81*, 1917–1926.

Hansel, D., Mato, G., and Meunier, C. (1993). Phase dynamics for weakly coupled Hodgkin-Huxley neurons. Europhys. Lett. *23*, 367–372.

Harraz, O.F., Longden, T.A., Dabertrand, F., Hill-Eubanks, D., and Nelson, M.T. (2018). Endothelial GqPCR activity controls capillary electrical signaling and brain blood flow through PIP_2 depletion. Proc. Natl. Acad. Sci. USA *115*, E3569–E3577.

He, B.J., and Raichle, M.E. (2009). The fMRI signal, slow cortical potential and consciousness. Trends Cogn. Sci. *13*, 302–309.

He, Y., Wang, M., Chen, X., Pohmann, R., Polimeni, J.R., Scheffler, K., Rosen, B.R., Kleinfeld, D., and Yu, X. (2018). Ultra-slow single-vessel BOLD and CBV-based fMRI spatiotemporal dynamics and their correlation with neuronal intracellular calcium signals. Neuron *97*, 925–939.e5.

Held, D., Fencl, V., and Pappenheimer, J.R. (1964). Electrical properties of cerebralspina; fluid. J. Neurophysiol. *27*, 942–959.

Hillman, E.M. (2014). Coupling mechanism and significance of the BOLD signal: a status report. Annu. Rev. Neurosci. *37*, 161–181.

Honey, C.J., Sporns, O., Cammoun, L., Gigandet, X., Thiran, J.P., Meuli, R., and Hagmann, P. (2009). Predicting human resting-state functional connectivity from structural connectivity. Proc. Natl. Acad. Sci. USA *106*, 2035–2040.

Horovitz, S.G., Fukunaga, M., de Zwart, J.A., van Gelderen, P., Fulton, S.C., Balkin, T.J., and Duyn, J.H. (2008). Low frequency BOLD fluctuations during resting wakefulness and light sleep: a simultaneous EEG-fMRI study. Hum. Brain Mapp. *29*, 671–682.

Hotta, H., Masamoto, K., Uchida, S., Sekiguchi, Y., Takuwa, H., Kawaguchi, H., Shigemoto, K., Sudo, R., Tanishita, K., Ito, H., and Kanno, I. (2013). Layer-specific dilation of penetrating arteries induced by stimulation of the nucleus basalis of Meynert in the mouse frontal cortex. J. Cereb. Blood Flow Metab. *33*, 1440–1447.

Hu, X., Le, T.H., Parrish, T., and Erhard, P. (1995). Retrospective estimation and correction of physiological fluctuation in functional MRI. Magn. Reson. Med. *34*, 201–212.

Huber, L., Handwerker, D.A., Jangraw, D.C., Chen, G., Hall, A., Stüber, C., Gonzalez-Castillo, J., Ivanov, D., Marrett, S., Guidi, M., et al. (2017). High-resolution CBV-fMRI allows mapping of laminar activity and connectivity of cortical Input and output in human M1. Neuron *96*, 1253–1263.e7.

Huo, B.X., Smith, J.B., and Drew, P.J. (2014). Neurovascular coupling and decoupling in the cortex during voluntary locomotion. J. Neurosci. *34*, 10975–10981.

Huo, B.X., Gao, Y.R., and Drew, P.J. (2015). Quantitative separation of arterial and venous cerebral blood volume increases during voluntary locomotion. Neuroimage *105*, 369–379.

Huppé-Gourgues, F., Jegouic, K., and Vaucher, E. (2018). Topographic organization of cholinergic innervation From the basal forebrain to the visual cortex in the rat. Front. Neural Circuits *12*, 19.

Iaccarino, H.F., Singer, A.C., Martorell, A.J., Rudenko, A., Gao, F., Gillingham, T.Z., Mathys, H., Seo, J., Kritskiy, O., Abdurrob, F., et al. (2016). Gamma frequency entrainment attenuates amyloid load and modifies microglia. Nature *540*, 230–235.

Iadecola, C. (2004). Neurovascular regulation in the normal brain and in Alzheimer's disease. Nat. Rev. Neurosci. *5*, 347–360.

Ichikawa, N., Fujiwara, M., Kawaguchi, F., Kaga, M., and Kawasak, S. (1999). Development of optical topography system ETG-100. Dedix Report *34*, 47–52.

Ilch, C.P., and Golanov, E.V. (2004). Cerebrovasodilation evoked by stimulation of subthalamic vasodilator area and hypoxia depends upon the integrity of cortical neurons in the rat. Neurosci. Lett. *368*, 92–95.

Iliff, J.J., Wang, M., Liao, Y., Plogg, B.A., Peng, W., Gundersen, G.A., Benveniste, H., Vates, G.E., Deane, R., Goldman, S.A., et al. (2012). A paravascular pathway facilitates CSF flow through the brain parenchyma and the clearance of interstitial solutes, including amyloid β. Sci. Transl. Med. *4*, 147ra111.

Intaglietta, M. (1990). Vasomotion and flowmotion: physiological mechanisms and clinical evidence. Vascular Medicine Review *1*, 101–112.

Kaminer, J., Powers, A.S., Horn, K.G., Hui, C., and Evinger, C. (2011). Characterizing the spontaneous blink generator: an animal model. J. Neurosci. *31*, 11256–11267.

Kay, K.N., Naselaris, T., Prenger, R.J., and Gallant, J.L. (2008). Identifying natural images from human brain activity. Nature *452*, 352–355.

Keller, C.J., Bickel, S., Honey, C.J., Groppe, D.M., Entz, L., Craddock, R.C., Lado, F.A., Kelly, C., Milham, M., and Mehta, A.D. (2013). Neurophysiological investigation of spontaneous correlated and anticorrelated fluctuations of the BOLD signal. J. Neurosci. *33*, 6333–6342.

Kim, J.H., Jung, A.H., Jeong, D., Choi, I., Kim, K., Shin, S., Kim, S.J., and Lee, S.-H. (2016a). Selectivity of neuromodulatory projections from the basal forebrain and locus ceruleus to primary sensory cortices. J. Neurosci. *36*, 5314–5327.

Kim, K.J., Ramiro Diaz, J., Iddings, J.A., and Filosa, J.A. (2016b). Vasculo-neuronal coupling: Retrograde vascular communication to brain neurons. J. Neurosci. *36*, 12624–12639.

Kim, Y., Yang, G.R., Pradhan, K., Venkataraju, K.U., Bota, M., García Del Molino, L.C., Fitzgerald, G., Ram, K., He, M., Levine, J.M., et al. (2017). Brain-wide maps reveal stereotyped cell-type-based cortical architecture and subcortical sexual dimorphism. Cell *171*, 456–469.e22.

Kiviniemi, V., Ruohonen, J., and Tervonen, O. (2005). Separation of physiological very low frequency fluctuation from aliasing by switched sampling interval fMRI scans. Magn. Reson. Imaging *23*, 41–46.

Kleinfeld, D., Mitra, P.P., Helmchen, F., and Denk, W. (1998). Fluctuations and stimulus-induced changes in blood flow observed in individual capillaries in layers 2 through 4 of rat neocortex. Proc. Natl. Acad. Sci. USA *95*, 15741–15746.

Kleinfeld, D., Blinder, P., Drew, P.J., Driscoll, J.D., Muller, A., Tsai, P.S., and Shih, A.Y. (2011). A guide to delineate the logic of neurovascular signaling in the brain. Front. Neuroenergetics *3*, 1–9.

Knot, H.J., and Nelson, M.T. (1998). Regulation of arterial diameter and wall [Ca^{2+}] in cerebral arteries of rat by membrane potential and intravascular pressure. J. Physiol. *508*, 199–209.

Knutsen, P.M., Mateo, C., and Kleinfeld, D. (2016). Precision mapping of the vibrissa representation within murine primary somatosensory cortex. Philos. Trans. R. Soc. Lond. B Biol. Sci. *371*, e20150351.

Koenigsberger, M., Sauser, R., Bény, J.-L., and Meister, J.-J. (2006). Effects of arterial wall stress on vasomotion. Biophys. J. *91*, 1663–1674.

Kopell, N., and LeMasson, G. (1994). Rhythmogenesis, amplitude modulation, and multiplexing in a cortical architecture. Proc. Natl. Acad. Sci. USA *91*, 10586–10590.

Koukouli, F., Rooy, M., Changeux, J.-P., and Maskos, U. (2016). Nicotinic receptors in mouse prefrontal cortex modulate ultraslow fluctuations related to conscious processing. Proc. Natl. Acad. Sci. USA *113*, 14823–14828.

Krawchuk, M.B., Ruff, C.F., Yang, X., Ross, S.E., and Vazquez, A.L. (2019). Optogenetic assessment of VIP, PV, SOM and NOS inhibitory neuron activity and cerebral blood flow regulation in mouse somato-sensory cortex. J. Cereb. Blood Flow Metab. *40*, 1427–1440.

Kuramoto, Y. (1984). Chemical Oscillations, Waves and Turbulence (Springer Verlag).

Kurnikova, A., Moore, J.D., Liao, S.-M., Deschênes, M., and Kleinfeld, D. (2017). Coordination of orofacial motor actions into exploratory behavior by rat. Curr. Biol. *27*, 688–696.

Kwong, K.K., Belliveau, J.W., Chesler, D.A., Goldberg, I.E., Weisskoff, R.M., Poncelet, B.P., Kennedy, D.N., Hoppel, B.E., Cohen, M.S., Turner, R., et al. (1992). Dynamic magnetic resonance imaging of human brain activity during primary sensory stimulation. Proc. Natl. Acad. Sci. USA *89*, 5675–5679.

Lachaux, J.-P., Fonlupt, P., Kahane, P., Minotti, L., Hoffmann, D., Bertrand, O., and Baciu, M. (2007). Relationship between task-related gamma oscillations and BOLD signal: new insights from combined fMRI and intracranial EEG. Hum. Brain Mapp. *28*, 1368–1375.

Laird, A.R., Lancaster, J.L., and Fox, P.T. (2005). BrainMap: the social evolution of a human brain mapping database. Neuroinformatics *3*, 65–78.

Lear, C.S.C., Flanagan, J.B., Jr., and Moorrees, C.F.A. (1965). The frequency of deglutition in man. Arch. Oral Biol. *10*, 83–100.

Lee, J.H., Durand, R., Gradinaru, V., Zhang, F., Goshen, I., Kim, D.S., Fenno, L.E., Ramakrishnan, C., and Deisseroth, K. (2010). Global and local fMRI signals driven by neurons defined optogenetically by type and wiring. Nature *465*, 788–792.

Lemon, R. (1984). Methods for Neuronal Recording in Conscious Animals (John Wiley and Sons).

Leopold, D.A., Murayama, Y., and Logothetis, N.K. (2003). Very slow activity fluctuations in monkey visual cortex: implications for functional brain imaging. Cereb. Cortex *13*, 422–433.

Li, N., Daie, K., Svoboda, K., and Druckmann, S. (2016). Robust neuronal dynamics in premotor cortex during motor planning. Nature *532*, 459–464.

Li, X., Yu, B., Sun, Q., Zhang, Y., Ren, M., Zhang, X., Li, A., Yuan, J., Madisen, L., Luo, Q., et al. (2018). Generation of a whole-brain atlas for the cholinergic system and mesoscopic projectome analysis of basal forebrain cholinergic neurons. Proc. Natl. Acad. Sci. USA *115*, 415–420.

Liang, Z., Liu, X., and Zhang, N. (2015). Dynamic resting state functional connectivity in awake and anesthetized rodents. Neuroimage *104*, 89–99.

Lieke, E.E., Frostig, R.D., Arieli, A., Ts'o, D.Y., Hildesheim, R., and Grinvald, A. (1989). Optical imaging of cortical activity: real-time imaging using extrinsic dye-signals and high resolution imaging based on slow intrinsic-signals. Annu. Rev. Physiol. *51*, 543–559.

Lima, B., Cardoso, M.M., Sirotin, Y.B., and Das, A. (2014). Stimulus-related neuroimaging in task-engaged subjects is best predicted by concurrent spiking. J. Neurosci. *34*, 13878–13891.

Lindauer, U., Megow, D., Matsuda, H., and Dirnagl, U. (1999). Nitric oxide: a modulator, but not a mediator, of neurovascular coupling in rat somatosensory cortex. Am. J. Physiol. *277*, H799–H811.

Liu, X., and Duyn, J.H. (2013). Time-varying functional network information extracted from brief instances of spontaneous brain activity. Proc. Natl. Acad. Sci. USA *110*, 4392–4397.

Liu, X., de Zwart, J.A., Schölvinck, M.L., Chang, C., Ye, F.Q., Leopold, D.A., and Duyn, J.H. (2018). Subcortical evidence for a contribution of arousal to fMRI studies of brain activity. Nat. Commun. *9*, 395.

Logothetis, N.K., and Wandell, B.A. (2004). Interpreting the BOLD signal. Annu. Rev. Physiol. *66*, 735–769.

Logothetis, N.K., Pauls, J., Augath, M., Trinath, T., and Oeltermann, A. (2001). Neurophysiological investigation of the basis of the fMRI signal. Nature *412*, 150–157.

Logothetis, N.K., Eschenko, O., Murayama, Y., Augath, M., Steudel, T., Evrard, H.C., Besserve, M., and Oeltermann, A. (2012). Hippocampal-cortical interaction during periods of subcortical silence. Nature *491*, 547–553.

Longden, T.A., Dabertrand, F., Koide, M., Gonzales, A.L., Tykocki, N.R., Brayden, J.E., Hill-Eubanks, D., and Nelson, M.T. (2017). Capillary K^+-sensing initiates retrograde hyperpolarization to increase local cerebral blood flow. Nat. Neurosci. *20*, 717–726.

Lowe, M.J., Mock, B.J., and Sorenson, J.A. (1998). Functional connectivity in single and multislice echoplanar imaging using resting-state fluctuations. Neuroimage *7*, 119–132.

Lowen, S.B., Cash, S.S., Poo, M., and Teich, M.C. (1997). Quantal neurotransmitter secretion rate exhibits fractal behavior. J. Neurosci. *17*, 5666–5677.

Lu, H., Golay, X., Pekar, J.J., and Van Zijl, P.C. (2003). Functional magnetic resonance imaging based on changes in vascular space occupancy. Magn. Reson. Med. *50*, 263–274.

Lu, H., Zou, Q., Gu, H., Raichle, M.E., Stein, E.A., and Yang, Y. (2012). Rat brains also have a default mode network. Proc. Natl. Acad. Sci. USA *109*, 3979–3984.

Lv, Y., Margulies, D.S., Cameron Craddock, R., Long, X., Winter, B., Gierhake, D., Endres, M., Villringer, K., Fiebach, J., and Villringer, A. (2013). Identifying the perfusion deficit in acute stroke with resting-state functional magnetic resonance imaging. Ann. Neurol. *73*, 136–140.

Ma, J., Ayata, C., Huang, P.L., Fishman, M.C., and Moskowitz, M.A. (1996). Regional cerebral blood flow response to vibrissal stimulation in mice lacking type I NOS gene expression. Am. J. Physiol. *270*, H1085–H1090.

Ma, Y., Shaik, M.A., Kozberg, M.G., Kim, S.H., Portes, J.P., Timerman, D., and Hillman, E.M. (2016). Resting-state hemodynamics are spatiotemporally coupled to synchronized and symmetric neural activity in excitatory neurons. Proc. Natl. Acad. Sci. USA *113*, E8463–E8471.

Majeed, W., Magnuson, M., Hasenkamp, W., Schwarb, H., Schumacher, E.H., Barsalou, L., and Keilholz, S.D. (2011). Spatiotemporal dynamics of low frequency BOLD fluctuations in rats and humans. Neuroimage *54*, 1140–1150.

Martin, R.E., Goodyear, B.G., Gati, J.S., and Menon, R.S. (2001). Cerebral cortical representation of automatic and volitional swallowing in humans. J. Neurophysiol. *85*, 938–950.

Mateo, C., Knutsen, P.M., Tsai, P.S., Shih, A.Y., and Kleinfeld, D. (2017). Entrainment of arteriole vasomotor fluctuations by neural activity is a basis of blood-oxygenation-level-dependent "resting state" connectivity. Neuron *96*, 936–948.e3.

Mathiisen, T.M., Lehre, K.P., Danbolt, N.C., and Ottersen, O.P. (2010). The perivascular astroglial sheath provides a complete covering of the brain microvessels: an electron microscopic 3D reconstruction. Glia *58*, 1094–1103.

Mathis, A., Mamidanna, P., Cury, K.M., Abe, T., Murthy, V.N., Mathis, M.W., and Bethge, M. (2018). DeepLabCut: markerless pose estimation of user-defined body parts with deep learning. Nat. Neurosci. *21*, 1281–1289.

Mayhew, J.E.W., Askew, S., Zheng, Y., Porrill, J., Westby, G.W.M., Redgrave, P., Rector, D.M., and Harper, R.M. (1996). Cerebral vasomotion: a 0.1-Hz oscillation in reflected light imaging of neural activity. Neuroimage *4*, 183–193.

Mishra, A., Reynolds, J.P., Chen, Y., Gourine, A.V., Rusakov, D.A., and Attwell, D. (2016). Astrocytes mediate neurovascular signaling to capillary pericytes but not to arterioles. Nat. Neurosci. *19*, 1619–1627.

Mitra, P.P. (2014). The circuit architecture of whole brains at the mesoscopic scale. Neuron *83*, 1273–1283.

Mitra, P.P., and Bokil, H.S. (2008). Observed Brain Dynamics (Oxford University Press).

Mitra, P.P., Ogawa, S., Hu, X., and Uğurbil, K. (1997). The nature of spatiotemporal changes in cerebral hemodynamics as manifested in functional magnetic resonance imaging. Magn. Reson. Med. *37*, 511–518.

Mitra, A., Snyder, A.Z., Blazey, T., and Raichle, M.E. (2015). Lag threads organize the brain's intrinsic activity. Proc. Natl. Acad. Sci. USA *112*, E2235–E2244.

Mohajerani, M.H., McVea, D.A., Fingas, M., and Murphy, T.H. (2010). Mirrored bilateral slow-wave cortical activity within local circuits revealed by fast bihemispheric voltage-sensitive dye imaging in anesthetized and awake mice. J. Neurosci. *30*, 3745–3751.

Mohajerani, M.H., Chan, A.W., Mohsenvand, M., LeDue, J., Liu, R., McVea, D.A., Boyd, J.D., Wang, Y.T., Reimers, M., and Murphy, T.H. (2013). Spontaneous cortical activity alternates between motifs defined by regional axonal projections. Nat. Neurosci. *16*, 1426–1435.

Moon, C.H., Fukuda, M., and Kim, S.G. (2013). Spatiotemporal characteristics and vascular sources of neural-specific and -nonspecific fMRI signals at submillimeter columnar resolution. Neuroimage *64*, 91–103.

Moshkforoush, A., Ashenagar, B., Harraz, O.F., Dabertrand, F., Longden, T.A., Nelson, M.T., and Tsoukias, N.M. (2020). The capillary Kir channel as sensor and amplifier of neuronal signals: Modeling insights on K^+-mediated neurovascular communication. Proceedings of the National Academy of Sciences USA *117*, 16626–16637.

Murphy, K., Birn, R.M., and Bandettini, P.A. (2013). Resting-state fMRI confounds and cleanup. Neuroimage *80*, 349–359.

Musall, S., Kaufman, M.T., Juavinett, A.L., Gluf, S., and Churchland, A.K. (2019). Single-trial neural dynamics are dominated by richly varied movements. Nat. Neurosci. *22*, 1677–1686.

Nakano, T., Kato, M., Morito, Y., Itoi, S., and Kitazawa, S. (2013). Blink-related momentary activation of the default mode network while viewing videos. Proc. Natl. Acad. Sci. USA *110*, 702–706.

Ngai, A.C., and Winn, H.R. (1996). Estimation of shear and flow rates in pial arterioles during somatosensory stimulation. Am. J. Physiol. *270*, H1712–H1717.

Niessing, J., Ebisch, B., Schmidt, K.E., Niessing, M., Singer, W., and Galuske, R.A. (2005). Hemodynamic signals correlate tightly with synchronized gamma oscillations. Science *309*, 948–951.

Nir, Y., Fisch, L., Mukamel, R., Gelbard-Sagiv, H., Arieli, A., Fried, I., and Malach, R. (2007). Coupling between neuronal firing rate, gamma LFP, and BOLD fMRI is related to interneuronal correlations. Curr. Biol. *17*, 1275–1285.

Nir, Y., Mukamel, R., Dinstein, I., Privman, E., Harel, M., Fisch, L., Gelbard-Sagiv, H., Kipervasser, S., Andelman, F., Neufeld, M.Y., et al. (2008). Interhemispheric correlations of slow spontaneous neuronal fluctuations revealed in human sensory cortex. Nat. Neurosci. *11*, 1100–1108.

Nita, D.A., Vanhatalo, S., Lafortune, F.-D., Voipio, J., Kaila, K., and Amzica, F. (2004). Nonneuronal origin of CO_2-related DC EEG shifts: an in vivo study in the cat. J. Neurophysiol. *92*, 1011–1022.

Nizar, K., Uhlirova, H., Tian, P., Saisan, P.A., Cheng, Q., Reznichenko, L., Weldy, K.L., Steed, T.C., Sridhar, V.B., MacDonald, C.L., et al. (2013). In vivo stimulus-induced vasodilation occurs without IP3 receptor activation and may precede astrocytic calcium increase. J. Neurosci. *33*, 8411–8422.

Noordmans, H.J., van Blooijs, D., Siero, J.C.W., Zwanenburg, J.J.M., Klaessens, J.H.G.M., and Ramsey, N.F. (2018). Detailed view on slow sinusoidal, hemodynamic oscillations on the human brain cortex by Fourier transforming oxy/deoxy hyperspectral images. Hum. Brain Mapp. *39*, 3558–3573.

Obrig, H., Neufang, M., Wenzel, R., Kohl, M., Steinbrink, J., Einhäupl, K., and Villringer, A. (2000). Spontaneous low frequency oscillations of cerebral hemodynamics and metabolism in human adults. Neuroimage *12*, 623–639.

Ogawa, S., Lee, T.-M., Nayak, A.S., and Glynn, P. (1990). Oxygenation-sensitive contrast in magnetic resonance image of rodent brain at high magnetic fields. Magn. Reson. Med. *14*, 68–78.

Ogawa, S., Tank, D.W., Menon, R., Ellermann, J.M., Kim, S.-G., Merkle, H., and Ugurbil, K. (1992). Intrinsic signal changes accompanying sensory stimulation: functional brain mapping with magnetic resonance imaging. Proc. Natl. Acad. Sci. USA *89*, 5951–5955.

Ogawa, S., Menon, R.S., Tank, D.W., Kim, S.G., Merkle, H., Ellermann, J.M., and Ugurbil, K. (1993). Functional brain mapping by blood oxygenation level-dependent contrast magnetic resonance imaging. A comparison of signal characteristics with a biophysical model. Biophys. J. *64*, 803–812.

Okun, M., Steinmetz, N.A., Lak, A., Dervinis, M., and Harris, K.D. (2019). Distinct structure of cortical population activity on fast and infraslow timescales. Cereb. Cortex *29*, 2196–2210.

Osol, G., and Halpern, W. (1988). Spontaneous vasomotion in pressurized cerebral arteries from genetically hypertensive rats. Am. J. Physiol. *254*, H28–H33.

Pais-Roldán, P., Biswal, B., Scheffler, K., and Yu, X. (2018). Identifying respiration-related aliasing artifacts in the rodent resting-state fMRI. Front. Neurosci. *12*, 788.

Pan, W.J., Billings, J.C., Grooms, J.K., Shakil, S., and Keilholz, S.D. (2015). Considerations for resting state functional MRI and functional connectivity studies in rodents. Front. Neurosci. *9*, 269.

Papoulis, A. (1962). The Fourier integral and its applications (McGraw-Hill Book Company).

Pauling, L., and Coryell, C.D. (1936). The magnetic properties and structure of hemoglobin, oxyhemoglobin and carbonmonoxyhemoglobin. Proc. Natl. Acad. Sci. USA *22*, 210–216.

Petridou, N., Gaudes, C.C., Dryden, I.L., Francis, S.T., and Gowland, P.A. (2013). Periods of rest in fMRI contain individual spontaneous events which are related to slowly fluctuating spontaneous activity. Hum. Brain Mapp. *34*, 1319–1329.

Pinto, L., Goard, M.J., Estandian, D., Xu, M., Kwan, A.C., Lee, S.H., Harrison, T.C., Feng, G., and Dan, Y. (2013). Fast modulation of visual perception by basal forebrain cholinergic neurons. Nat. Neurosci. *16*, 1857–1863.

Pisauro, M.A., Dhruv, N.T., Carandini, M., and Benucci, A. (2013). Fast hemodynamic responses in the visual cortex of the awake mouse. J. Neurosci. *33*, 18343–18351.

Poplawsky, A.J., Fukuda, M., Kang, B.M., Kim, J.H., Suh, M., and Kim, S.G. (2019). Dominance of layer-specific microvessel dilation in contrast-enhanced high-resolution fMRI: Comparison between hemodynamic spread and vascular architecture with CLARITY. Neuroimage *197*, 657–667.

Power, J.D., Barnes, K.A., Snyder, A.Z., Schlaggar, B.L., and Petersen, S.E. (2012). Spurious but systematic correlations in functional connectivity MRI networks arise from subject motion. Neuroimage *59*, 2142–2154.

Quigley, M., Cordes, D., Turski, P., Moritz, C., Haughton, V., Seth, R., and Meyerand, M.E. (2003). Role of the corpus callosum in functional connectivity. AJNR Am. J. Neuroradiol. *24*, 208–212.

Raichle, M.E., MacLeod, A.M., Snyder, A.Z., Powers, W.J., Gusnard, D.A., and Shulman, G.L. (2001). A default mode of brain function. Proc. Natl. Acad. Sci. USA *98*, 676–682.

Raj, D., Paley, D.P., Anderson, A.W., Kennan, R.P., and Gore, J.C. (2000). A model for susceptibility artefacts from respiration in functional echo-planar magnetic resonance imaging. Phys. Med. Biol. *45*, 3809–3820.

Rasmussen, R., Nicholas, E., Petersen, N.C., Dietz, A.G., Xu, Q., Sun, Q., and Nedergaard, M. (2019). Cortex-wide changes in extracellular potassium ions parallel brain state transitions in awake behaving mice. Cell Rep. *28*, 1182–1194.e4.

Rayshubskiy, A., Wojtasiewicz, T.J., Mikell, C.B., Bouchard, M.B., Timerman, D., Youngerman, B.E., McGovern, R.A., Otten, M.L., Canoll, P., McKhann, G.M., 2nd, and Hillman, E.M. (2014). Direct, intraoperative observation of ~0.1 Hz hemodynamic oscillations in awake human cortex: implications for fMRI. Neuroimage *87*, 323–331.

Reimer, J., Froudarakis, E., Cadwell, C.R., Yatsenko, D., Denfield, G.H., and Tolias, A.S. (2014). Pupil fluctuations track fast switching of cortical states during quiet wakefulness. Neuron *84*, 355–362.

Rennels, M.L., Gregory, T.F., Blaumanis, O.R., Fujimoto, K., and Grady, P.A. (1985). Evidence for a 'paravascular' fluid circulation in the mammalian central nervous system, provided by the rapid distribution of tracer protein throughout the brain from the subarachnoid space. Brain Res. *326*, 47–63.

Revel, A., Gallet, C., Oréa, V., Chapuis, B., Barrès, C., and Julien, C. (2012). Effect of chronic cervical ganglionectomy on the spontaneous variability of internal carotid blood flow in the conscious rat. Exp. Physiol. *97*, 564–571.

Rosenegger, D.G., Tran, C.H., Wamsteeker Cusulin, J.I., and Gordon, G.R. (2015). Tonic local brain blood flow control by astrocytes independent of phasic neurovascular coupling. J. Neurosci. *35*, 13463–13474.

Sakaguchi, H., Shinomoto, S., and Kuramoto, Y. (1988). Mutual entrainment in oscillator lattices with nonvariational type interaction. Prog. Theor. Phys. *79*, 1069–1079.

Salkoff, D.B., Zagha, E., McCarthy, E., and McCormick, D.A. (2019). Movement and performance explain widespread cortical activity in a visual detection task. Cereb. Cortex *30*, 421–437.

Saper, C.B. (1984). Organization of cerebral cortical afferent systems in the rat. II. Magnocellular basal nucleus. J. Comp. Neurol. *222*, 313–342.

Sato, A., Sato, Y., and Uchida, S. (2001). Regulation of regional cerebral blood flow by cholinergic fibers originating in the basal forebrain. Int. J. Dev. Neurosci. *19*, 327–337.

Schölvinck, M.L., Maier, A., Ye, F.Q., Duyn, J.H., and Leopold, D.A. (2010). Neural basis of global resting-state fMRI activity. Proc. Natl. Acad. Sci. USA *107*, 10238–10243.

Schölvinck, M.L., Saleem, A.B., Benucci, A., Harris, K.D., and Carandini, M. (2015). Cortical state determines global variability and correlations in visual cortex. J. Neurosci. *35*, 170–178.

Schulz, K., Sydekum, E., Krueppel, R., Engelbrecht, C.J., Schlegel, F., Schröter, A., Rudin, M., and Helmchen, F. (2012). Simultaneous BOLD fMRI and fiber-optic calcium recording in rat neocortex. Nat. Methods *9*, 597–602.

Schwalm, M., Schmid, F., Wachsmuth, L., Backhaus, H., Kronfeld, A., Aedo Jury, F., Prouvot, P.H., Fois, C., Albers, F., van Alst, T., et al. (2017). Cortex-wide BOLD fMRI activity reflects locally-recorded slow oscillation-associated calcium waves. eLife *6*, e27602.

Segal, S.S., and Duling, B.R. (1989). Conduction of vasomotor responses in arterioles: a role for cell-to-cell coupling? Am. J. Physiol. *256*, H838–H845.

Semba, K., Reiner, P.B., McGeer, E.G., and Fibiger, H.C. (1988). Non-cholinergic basal forebrain neurons project to the contralateral basal forebrain in the rat. Neurosci. Lett. *84*, 23–28.

Şencan, I., Esipova, T., Kılıç, K., Li, B., Desjardins, M., Yaseen, M.A., Wang, H., Porter, J.E., Kura, S., Fu, B., et al. (2020). Optical measurement of microvascular oxygenation and blood flow responses in awake mouse cortex during functional activation. J. Cereb. Blood Flow Metab. Published online June 9, 2020. https://doi.org/10.1177/0271678X20928011.

Shmuel, A., and Leopold, D.A. (2008). Neuronal correlates of spontaneous fluctuations in fMRI signals in monkey visual cortex: Implications for functional connectivity at rest. Hum. Brain Mapp. *29*, 751–761.

Shmuel, A., Augath, M., Oeltermann, A., and Logothetis, N.K. (2006). Negative functional MRI response correlates with decreases in neuronal activity in monkey visual area V1. Nat. Neurosci. *9*, 569–577.

Shmueli, K., van Gelderen, P., de Zwart, J.A., Horovitz, S.G., Fukunaga, M., Jansma, J.M., and Duyn, J.H. (2007). Low-frequency fluctuations in the cardiac rate as a source of variance in the resting-state fMRI BOLD signal. Neuroimage *38*, 306–320.

Shulman, R.G., Hyder, F., and Rothman, D.L. (2002). Biophysical basis of brain activity: implications for neuroimaging. Q. Rev. Biophys. *35*, 287–325.

Siegel, J.S., Power, J.D., Dubis, J.W., Vogel, A.C., Church, J.A., Schlaggar, B.L., and Petersen, S.E. (2014). Statistical improvements in functional magnetic resonance imaging analyses produced by censoring high-motion data points. Hum. Brain Mapp. *35*, 1981–1996.

Sirotin, Y.B., Hillman, E.M., Bordier, C., and Das, A. (2009). Spatiotemporal precision and hemodynamic mechanism of optical point spreads in alert primates. Proc. Natl. Acad. Sci. USA *106*, 18390–18395.

Smith, S.M., Fox, P.T., Miller, K.L., Glahn, D.C., Fox, P.M., Mackay, C.E., Filippini, N., Watkins, K.E., Toro, R., Laird, A.R., and Beckmann, C.F. (2009). Correspondence of the brain's functional architecture during activation and rest. Proc. Natl. Acad. Sci. USA *106*, 13040–13045.

Sofroniew, N.J., Flickinger, D., King, J., and Svoboda, K. (2016). A large field of view two-photon mesoscope with subcellular resolution for in vivo imaging. eLife *5*, e14472.

Sohal, V.S., Zhang, F., Yizhar, O., and Deisseroth, K. (2009). Parvalbumin neurons and gamma rhythms enhance cortical circuit performance. Nature *459*, 698–702.

Sompolinsky, H., Golomb, D., and Kleinfeld, D. (1991). Cooperative dynamics in visual processing. Phys. Rev. A *43*, 6990–7011.

Sorensen, S.C., and Severinghaus, J.W. (1970). Effect of cerebral acidosis on the CSF-blood potential difference. Am. J. Physiol. *219*, 68–71.

Sporns, O., Tononi, G., and Kötter, R. (2005). The human connectome: A structural description of the human brain. PLoS Comput. Biol. *1*, e42.

Stafford, J.M., Jarrett, B.R., Miranda-Dominguez, O., Mills, B.D., Cain, N., Mihalas, S., Lahvis, G.P., Lattal, K.M., Mitchell, S.H., David, S.V., et al. (2014). Large-scale topology and the default mode network in the mouse connectome. Proc. Natl. Acad. Sci. USA *111*, 18745–18750.

Steinbrink, J., Villringer, A., Kempf, F., Haux, D., Boden, S., and Obrig, H. (2006). Illuminating the BOLD signal: combined fMRI-fNIRS studies. Magn. Reson. Imaging *24*, 495–505.

Steinmetz, N.A., Buetfering, C., Lecoq, J., Lee, C.R., Peters, A.J., Jacobs, E.A.K., Coen, P., Ollerenshaw, D.R., Valley, M.T., de Vries, S.E.J., et al. (2017). Aberrant cortical activity in multiple GCaMP6-expressing transgenic mouse lines. eNeuro *4*, e0207.

Stephan, K.E., Harrison, L.M., Penny, W.D., and Friston, K.J. (2004). Biophysical models of fMRI responses. Curr. Opin. Neurobiol. *14*, 629–635.

Stergiopulos, N., Porret, C.-A., De Brouwer, S., and Meister, J.-J. (1998). Arterial vasomotion: effect of flow and evidence of nonlinear dynamics. Am. J. Physiol. *274*, H1858–H1864.

Steriade, M., Contreras, D., Curró Dossi, R., and Nuñez, A. (1993). The slow (< 1 Hz) oscillation in reticular thalamic and thalamocortical neurons: scenario of sleep rhythm generation in interacting thalamic and neocortical networks. J. Neurosci. *13*, 3284–3299.

Stringer, C., Pachitariu, M., Steinmetz, N., Reddy, C.B., Carandini, M., and Harris, K.D. (2019). Spontaneous behaviors drive multidimensional, brainwide activity. Science *364*, 255.

Strogatz, S.H., and Mirolla, R.E. (1988). Phase-locking and critical phenomena in lattices of coupled nonlinear oscillators with random intrinsic frequencies. Physica D *31*, 143–168.

Tagliazucchi, E., and Laufs, H. (2014). Decoding wakefulness levels from typical fMRI resting-state data reveals reliable drifts between wakefulness and sleep. Neuron *82*, 695–708.

Thompson, G.J., Merritt, M.D., Pan, W.-J., Magnuson, M.E., Grooms, J.K., Jaeger, D., and Keilholz, S.D. (2013). Neural correlates of time-varying functional connectivity in the rat. Neuroimage *83*, 826–836.

Thompson, G.J., Pan, W.J., Magnuson, M.E., Jaeger, D., and Keilholz, S.D. (2014). Quasi-periodic patterns (QPP): large-scale dynamics in resting state fMRI that correlate with local infraslow electrical activity. Neuroimage *84*, 1018–1031.

Tian, P., Teng, I.C., May, L.D., Kurz, R., Lu, K., Scadeng, M., Hillman, E.M., De Crespigny, A.J., D'Arceuil, H.E., Mandeville, J.B., et al. (2010). Cortical depth-specific microvascular dilation underlies laminar differences in blood oxygenation level-dependent functional MRI signal. Proc. Natl. Acad. Sci. USA *107*, 15246–15251.

Toib, A., Lyakhov, V., and Marom, S. (1998). Interaction between duration of activity and time course of recovery from slow inactivation in mammalian brain Na+ channels. J. Neurosci. *18*, 1893–1903.

Tong, Y., Hocke, L.M., Fan, X., Janes, A.C., and Frederick, Bd. (2015). Can apparent resting state connectivity arise from systemic fluctuations? Front. Hum. Neurosci. *9*, 285.

Tong, Y., Yao, J.F., Chen, J.J., and Frederick, B.D. (2019). The resting-state fMRI arterial signal predicts differential blood transit time through the brain. J. Cereb. Blood Flow Metab. *39*, 1148–1160.

Tsai, P.S., Mateo, C., Field, J.J., Schaffer, C.B., Anderson, M.E., and Kleinfeld, D. (2015). Ultra-large field-of-view two-photon microscopy. Opt. Express *23*, 13833–13847.

Tsitoura, C., Malinowski, S.T., Mohrhardt, J., Degen, R., DiBenedictis, B.T., Gao, Y., Watznauer, K., Gerhold, K., Nagel, M., Weber, M., et al. (2020). Synchronous infra-slow oscillations organize ensembles of accessory olfactory bulb projection neurons into distinct microcircuits. J. Neurosci. *40*, 4203–4218.

Turchi, J., Chang, C., Ye, F.Q., Russ, B.E., Yu, D.K., Cortes, C.R., Monosov, I.E., Duyn, J.H., and Leopold, D.A. (2018). The basal forebrain regulates global resting-state fMRI fluctuations. Neuron *97*, 940–952.e4.

Tyszka, J.M., Kennedy, D.P., Adolphs, R., and Paul, L.K. (2011). Intact bilateral resting-state networks in the absence of the corpus callosum. J. Neurosci. *31*, 15154–15162.

Uhlirova, H., Kılıç, K., Tian, P., Thunemann, M., Desjardins, M., Saisan, P.A., Sakadžić, S., Ness, T.V., Mateo, C., Cheng, Q., et al. (2016). Cell type specificity of neurovascular coupling in cerebral cortex. eLife *5*, e14315.

Uludağ, K., Müller-Bierl, B., and Uğurbil, K. (2009). An integrative model for neuronal activity-induced signal changes for gradient and spin echo functional imaging. Neuroimage *48*, 150–165.

Van de Moortele, P.F., Pfeuffer, J., Glover, G.H., Ugurbil, K., and Hu, X. (2002). Respiration-induced B0 fluctuations and their spatial distribution in the human brain at 7 Tesla. Magn. Reson. Med. *47*, 888–895.

van Gelderen, P., de Zwart, J.A., Starewicz, P., Hinks, R.S., and Duyn, J.H. (2007). Real-time shimming to compensate for respiration-induced B0 fluctuations. Magn. Reson. Med. *57*, 362–368.

van Veluw, S.J., Hou, S.S., Calvo-Rodriguez, M., Arbel-Ornath, M., Snyder, A.C., Frosch, M.P., Greenberg, S.M., and Bacskai, B.J. (2020). Vasomotion as a driving force for paravascular clearance in the awake mouse brain. Neuron *105*, 549–561.e5.

Van Vreeswijk, C., Abbott, L.F., and Ermentrout, G.B. (1994). When inhibition not excitation synchronizes neural firing. J. Comput. Neurosci. *1*, 313–321.

Vanhatalo, S., Tallgren, P., Becker, C., Holmes, M.D., Miller, J.W., Kaila, K., and Voipio, J. (2003). Scalp-recorded slow EEG responses generated in response to hemodynamic changes in the human brain. Clin. Neurophysiol. *114*, 1744–1754.

Vanni, M.P., Chan, A.W., Balbi, M., Silasi, G., and Murphy, T.H. (2017). Mesoscale mapping of mouse cortex reveals frequency-dependent cycling between distinct macroscale functional modules. J. Neurosci. *37*, 7513–7533.

Vaucher, E., and Hamel, E. (1995). Cholinergic basal forebrain neurons project to cortical microvessels in the rat: electron microscopic study with anterogradely transported Phaseolus vulgaris leucoagglutinin and choline acetyltransferase immunocytochemistry. J. Neurosci. *15*, 7427–7441.

Vazquez, A.L., Fukuda, M., and Kim, S.G. (2012). Evolution of the dynamic changes in functional cerebral oxidative metabolism from tissue mitochondria to blood oxygen. J. Cereb. Blood Flow Metab. *32*, 745–758.

Villringer, A., and Dirnagl, U. (1995). Coupling of brain activity and cerebral blood flow: basis of functional neuroimaging. Cerebrovasc. Brain Metab. Rev. *7*, 240–276.

Vincent, J.L., Patel, G.H., Fox, M.D., Snyder, A.Z., Baker, J.T., Van Essen, D.C., Zempel, J.M., Snyder, L.H., Corbetta, M., and Raichle, M.E. (2007). Intrinsic functional architecture in the anaesthetized monkey brain. Nature *447*, 83–86.

Voipio, J., Tallgren, P., Heinonen, E., Vanhatalo, S., and Kaila, K. (2003). Millivolt-scale DC shifts in the human scalp EEG: evidence for a nonneuronal generator. J. Neurophysiol. *89*, 2208–2214.

Wang, M., He, Y., Sejnowski, T.J., and Yu, X. (2018). Brain-state dependent astrocytic Ca(2+) signals are coupled to both positive and negative BOLD-fMRI signals. Proc. Natl. Acad. Sci. USA *115*, 1647–1656.

Welsh, D.G., Tran, C.H.T., Hald, B.O., and Sancho, M. (2018). The conducted vasomotor response: function, biophysical basis, and pharmacological control. Annu. Rev. Pharmacol. Toxicol. *58*, 391–410.

Whishaw, B.K., and Whishaw, I.Q. (2014). An introduction to brain and behavior (Worth Publishers).

White, J.A., Banks, M.I., Pearce, R.A., and Kopell, N.J. (2000). Networks of interneurons with fast and slow gamma-aminobutyric acid A (GABA-a) kinetics provide substrate for mixed gamma-theta rhythm. Proc. Natl. Acad. Sci. USA *97*, 8128–8133.

Whittington, M.A., Traub, R.D., and Jefferys, J.G. (1995). Synchronized oscillations in interneuron networks driven by metabotropic glutamate receptor activation. Nature *373*, 612–615.

Williams, K.A., Magnuson, M., Majeed, W., LaConte, S.M., Peltier, S.J., Hu, X., and Keilholz, S.D. (2010). Comparison of alpha-chloralose, medetomidine and isoflurane anesthesia for functional connectivity mapping in the rat. Magn. Reson. Imaging *28*, 995–1003.

Winder, A.T., Echagarruga, C., Zhang, Q., and Drew, P.J. (2017). Weak correlations between hemodynamic signals and ongoing neural activity during the resting state. Nat. Neurosci. *20*, 1761–1769.

Wise, R.G., Ide, K., Poulin, M.J., and Tracey, I. (2004). Resting fluctuations in arterial carbon dioxide induce significant low frequency variations in BOLD signal. Neuroimage *21*, 1652–1664.

Wu, H., Williams, J., and Nathans, J. (2014). Complete morphologies of basal forebrain cholinergic neurons in the mouse. eLife *3*, e02444.

Yamada, M., Lamping, K.G., Duttaroy, A., Zhang, W., Cui, Y., Bymaster, F.P., McKinzie, D.L., Felder, C.C., Deng, C.-X., Faraci, F.M., and Wess, J. (2001). Cholinergic dilation of cerebral blood vessels is abolished in M(5) muscarinic acetylcholine receptor knockout mice. Proc. Natl. Acad. Sci. USA *98*, 14096–14101.

Yan, C.G., Cheung, B., Kelly, C., Colcombe, S., Craddock, R.C., Di Martino, A., Li, Q., Zuo, X.-N., Castellanos, F.X., and Milham, M.P. (2013). A comprehensive assessment of regional variation in the impact of head micromovements on functional connectomics. Neuroimage *76*, 183–201.

Yeung, M.K.S., and Strogatz, S.H. (1999). Time delay in the Kuramoto model of coupled oscillators. Phys. Rev. Lett. *82*, 648–651.

Yu, X., Glen, D., Wang, S., Dodd, S., Hirano, Y., Saad, Z., Reynolds, R., Silva, A.C., and Koretsky, A.P. (2012). Direct imaging of macrovascular and microvascular contributions to BOLD fMRI in layers IV-V of the rat whisker-barrel cortex. Neuroimage *59*, 1451–1460.

Yu, X., Qian, C., Chen, D.Y., Dodd, S.J., and Koretsky, A.P. (2014). Deciphering laminar-specific neural inputs with line-scanning fMRI. Nat. Methods *11*, 55–58.

Yu, J., Gutnisky, D.A., Hires, S.A., and Svoboda, K. (2016). Layer 4 fast-spiking interneurons filter thalamocortical signals during active somatosensation. Nat. Neurosci. *19*, 1647–1657.

Yüzgeç, Ö., Prsa, M., Zimmermann, R., and Huber, D. (2018). Pupil size coupling to cortical states protects the stability of deep sleep via parasympathetic modulation. Curr. Biol. *28*, 392–400.e3.

Zaborszky, L., Csordas, A., Mosca, K., Kim, J., Gielow, M.R., Vadasz, C., and Nadasdy, Z. (2015). Neurons in the basal forebrain project to the cortex in a complex topographic organization that reflects corticocortical connectivity patterns: an experimental study based on retrograde tracing and 3D reconstruction. Cereb. Cortex *25*, 118–137.

Zeng, H. (2018). Mesoscale connectomics. Curr. Opin. Neurobiol. *50*, 154–162.

Zerbi, V., Floriou-Servou, A., Markicevic, M., Vermeiren, Y., Sturman, O., Privitera, M., von Ziegler, L., Ferrari, K.D., Weber, B., De Deyn, P.P., et al. (2019). Rapid reconfiguration of the functional connectome after chemogenetic locus coeruleus activation. Neuron *103*, 702–718.e5.

Zhang, Q., Roche, M., Gheres, K.W., Chaigneau, E., Kedarasetti, R.T., Haselden, W.D., Charpak, S., and Drew, P.J. (2019). Cerebral oxygenation during locomotion is modulated by respiration. Nat. Commun. *10*, 5515.

Zhao, F., Zhao, T., Zhou, L., Wu, Q., and Hu, X. (2008). BOLD study of stimulation-induced neural activity and resting-state connectivity in medetomidine-sedated rat. Neuroimage *39*, 248–260.